



This is a repository copy of *Low-latency gravitational-wave alerts for multimessenger astronomy during the second Advanced LIGO and Virgo observing run.*

White Rose Research Online URL for this paper:

<https://eprints.whiterose.ac.uk/213061/>

Version: Published Version

Article:

Abbott, B.P., Abbott, R., Abbott, T.D. et al. (1129 more authors) (2019) Low-latency gravitational-wave alerts for multimessenger astronomy during the second Advanced LIGO and Virgo observing run. *The Astrophysical Journal*, 875 (2). 161. ISSN 0004-637X

<https://doi.org/10.3847/1538-4357/ab0e8f>

Reuse

This article is distributed under the terms of the Creative Commons Attribution (CC BY) licence. This licence allows you to distribute, remix, tweak, and build upon the work, even commercially, as long as you credit the authors for the original work. More information and the full terms of the licence here:

<https://creativecommons.org/licenses/>

Takedown

If you consider content in White Rose Research Online to be in breach of UK law, please notify us by emailing eprints@whiterose.ac.uk including the URL of the record and the reason for the withdrawal request.



eprints@whiterose.ac.uk
<https://eprints.whiterose.ac.uk/>



Low-latency Gravitational-wave Alerts for Multimessenger Astronomy during the Second Advanced LIGO and Virgo Observing Run

B. P. Abbott¹, R. Abbott¹, T. D. Abbott², S. Abraham³, F. Acernese^{4,5}, K. Ackley⁶, C. Adams⁷, R. X. Adhikari¹, V. B. Adya^{8,9}, C. Affeldt^{8,9}, M. Agathos¹⁰, K. Agatsuma¹¹, N. Aggarwal¹², O. D. Aguiar¹³, L. Aiello^{14,15}, A. Ain³, P. Ajith¹⁶, G. Allen¹⁷, A. Allocca^{18,19}, M. A. Aloy²⁰, P. A. Altin²¹, A. Amato²², A. Ananyeva¹, S. B. Anderson¹, W. G. Anderson²³, S. V. Angelova²⁴, S. Antier²⁵, S. Appert¹, K. Arai¹, M. C. Araya¹, J. S. Areeda²⁶, M. Arène²⁷, N. Arnaud^{25,28}, S. Ascenzi^{29,30}, G. Ashton⁶, S. M. Aston⁷, P. Astone³¹, F. Aubin³², P. Aufmuth⁹, K. AultO'Neal³³, C. Austin², V. Avendano³⁴, A. Avila-Alvarez²⁶, S. Babak^{27,35}, P. Bacon²⁷, F. Badaracco^{14,15}, M. K. M. Bader³⁶, S. Bae³⁷, P. T. Baker³⁸, F. Baldaccini^{39,40}, G. Ballardin²⁸, S. W. Ballmer⁴¹, S. Banagiri⁴², J. C. Barayoga¹, S. E. Barclay⁴³, B. C. Barish¹, D. Barker⁴⁴, K. Barkett⁴⁵, S. Barnum¹², F. Barone^{4,5}, B. Barr⁴³, L. Barsotti¹², M. Barsuglia²⁷, D. Barta⁴⁶, J. Bartlett⁴⁴, I. Bartos⁴⁷, R. Bassiri⁴⁸, A. Basti^{18,19}, M. Bawaj^{40,49}, J. C. Bayley⁴³, M. Bazzan^{50,51}, B. Bécsy⁵², M. Bejger^{27,53}, I. Belahcene²⁵, A. S. Bell³, D. Beniwal⁵⁴, B. K. Berger⁴⁸, G. Bergmann^{8,9}, S. Bernuzzi^{55,56}, J. J. Bero⁵⁷, C. P. L. Berry⁵⁸, D. Bersanetti⁵⁹, A. Bertolini³⁶, J. Betzwieser⁷, R. Bhandare⁶⁰, J. Bidler²⁶, I. A. Bilenko⁶¹, S. A. Bilgili³⁸, G. Billingsley¹, J. Birch⁷, I. A. Birney²⁴, O. Birnholtz⁵⁷, S. Biscans^{1,12}, S. Biscoveanu⁶, A. Bisht⁹, M. Bitossi^{19,28}, M. A. Bizouard²⁵, J. K. Blackburn¹, C. D. Blair⁷, D. G. Blair⁶², R. M. Blair⁴⁴, S. Bloemen⁶³, N. Bode^{8,9}, M. Boer⁶⁴, Y. Boetzel⁶⁵, G. Bogaert⁶⁴, F. Bondu⁴⁸, E. Bonilla⁴⁸, R. Bonnand³², P. Booker^{8,9}, B. A. Boom³⁶, C. D. Booth⁶⁷, R. Bork¹, V. Boschi²⁸, S. Bose^{3,68}, K. Bossie⁷, V. Bossilkov⁶², J. Bosveld⁶², Y. Bouffanais²⁷, A. Bozzi²⁸, C. Bradaschia¹⁹, P. R. Brady²³, A. Bramley⁷, M. Branchesi^{14,15}, J. E. Brau⁶⁹, T. Briant⁷⁰, J. H. Briggs⁴³, F. Brighenti^{71,72}, A. Brillet⁶⁴, M. Brinkmann^{8,9}, V. Brisson^{25,178}, P. Brockill²³, A. F. Brooks¹, D. D. Brown⁵⁴, S. Brunetti¹, A. Buikema¹², T. Bulik⁷³, H. J. Bulten^{36,74}, A. Buonanno^{35,75}, D. Buskulic³², C. Buy²⁷, R. L. Byer⁴⁸, M. Cabero^{8,9}, L. Cadonati⁷⁶, G. Cagnoli^{22,77}, C. Cahillane¹, J. Calderón Bustillo⁶, T. A. Callister¹, E. Calloni^{5,78}, J. B. Camp⁷⁹, W. A. Campbell⁶, M. Canepa^{59,80}, K. C. Cannon⁸¹, H. Cao⁵⁴, J. Cao⁸², E. Capocasa²⁷, F. Carbognani²⁸, S. Caride⁸³, M. F. Carney⁵⁸, G. Carullo¹⁸, J. Casanueva Diaz¹⁹, C. Casentini^{29,30}, S. Caudill³⁶, M. Cavaglia⁸⁴, F. Cavalier²⁵, R. Cavalieri²⁸, G. Cella¹⁹, P. Cerdá-Durán²⁰, G. Cerretani^{18,19}, E. Cesarini^{30,85}, O. Chaibi⁶⁴, K. Chakravarti³, S. J. Chamberlin⁸⁶, M. Chan⁴³, S. Chao⁸⁷, P. Charlton⁸⁸, E. A. Chase⁵⁸, E. Chassande-Mottin²⁷, D. Chatterjee²³, M. Chaturvedi⁶⁰, B. D. Cheeseboro³⁸, H. Y. Chen⁸⁹, X. Chen⁶², Y. Chen⁴⁵, H.-P. Cheng⁴⁷, C. K. Cheong⁹⁰, H. Y. Chia⁴⁷, A. Chincarini⁵⁹, A. Chiummo²⁸, G. Cho⁹¹, H. S. Cho⁹², M. Cho⁷⁵, N. Christensen^{64,93}, Q. Chu⁶², S. Chua⁷⁰, K. W. Chung⁹⁰, S. Chung⁶², G. Ciani^{50,51}, A. A. Ciobanu⁵⁴, R. Ciolfi^{94,95}, F. Cipriano⁶⁴, A. Cirone^{59,80}, F. Clara⁴⁴, J. A. Clark⁷⁶, P. Clearwater⁹⁶, F. Cleva⁶⁴, C. Cocchieri⁸⁴, E. Coccia^{14,15}, P.-F. Cohadon⁷⁰, D. Cohen²⁵, R. Colgan⁹⁷, M. Colleoni⁹⁸, C. G. Collette⁹⁹, C. Collins¹¹, L. R. Cominsky¹⁰⁰, M. Constancio, Jr.¹³, L. Conti⁵¹, S. J. Cooper¹¹, P. Corban⁷, T. R. Corbitt², I. Cordero-Carrión¹⁰¹, K. R. Corley⁹⁷, N. Cornish⁵², A. Corsi⁸³, S. Cortese²⁸, C. A. Costa¹³, R. Cotesta³⁵, M. W. Coughlin¹, S. B. Coughlin^{58,67}, J.-P. Coulon⁶⁴, S. T. Countryman⁹⁷, P. Couvares¹, P. B. Covas⁹⁸, E. E. Cowan⁷⁶, D. M. Coward⁶², M. J. Cowart⁷, D. C. Coyne¹, R. Coyne¹⁰², J. D. E. Creighton²³, T. D. Creighton¹⁰³, J. Cripe², M. Croquette⁷⁰, S. G. Crowder¹⁰⁴, T. J. Cullen², A. Cumming⁴³, L. Cunningham⁴³, E. Cuoco²⁸, T. Dal Canton⁷⁹, G. Dálya¹⁰⁵, S. L. Danilishin^{8,9}, S. D'Antonio³⁰, K. Danzmann^{8,9}, A. Dasgupta¹⁰⁶, C. F. Da Silva Costa⁴⁷, L. E. H. Datrier⁴³, V. Dattilo⁸⁹, I. Dave⁶⁰, M. Davies²⁵, D. Davis⁴¹, E. J. Daw¹⁰⁷, D. DeBra⁴⁸, M. Deenadayan³, J. Degallaix²², M. De Laurentis^{5,78}, S. Deléglise⁷⁰, W. Del Pozzo^{18,19}, L. M. DeMarchi⁵⁸, N. Demos¹², T. Dent^{8,9,108}, R. De Pietri^{56,109}, J. Derby²⁶, R. De Rosa^{5,78}, C. De Rossi^{22,28}, R. DeSalvo¹¹⁰, O. de Varona^{8,9}, S. Dhurandhar³, M. C. Díaz¹⁰³, T. Dietrich³⁶, L. Di Fiore⁵, M. Di Giovanni^{95,111}, T. Di Girolamo^{5,78}, A. Di Lieto^{18,19}, B. Ding⁹⁹, S. Di Pace^{31,112}, I. Di Palma^{31,112}, F. Di Renzo^{18,19}, A. Dmitriev¹¹, Z. Doctor⁸⁹, F. Donovan¹², K. L. Dooley^{67,84}, S. Doravari^{8,9}, I. Dorrington⁶⁷, T. P. Downes²³, M. Drago^{14,15}, J. C. Driggers⁴⁴, Z. Du⁸², J.-G. Ducoin²⁵, P. Dupej⁴³, S. E. Dwyer⁴⁴, P. J. Easter⁶, T. B. Edo¹⁰⁷, M. C. Edwards⁹³, A. Effler⁷, P. Ehrens¹, J. Eichholz¹, S. S. Eikenberry⁴⁷, M. Eisenmann³², R. A. Eisenstein¹², R. C. Essick⁸⁹, H. Estelles⁹⁸, D. Estevez³², Z. B. Etienne³⁸, T. Etzel¹, M. Evans¹², T. M. Evans⁷, V. Fafone^{14,29,30}, H. Fair⁴¹, S. Fairhurst⁶⁷, X. Fan⁸², S. Farinon⁵⁹, B. Farr⁶⁹, W. M. Farr¹¹, E. J. Fauchon-Jones⁶⁷, M. Favata³⁴, M. Fays¹⁰⁷, M. Fazio¹¹³, C. Fee¹¹⁴, J. Feicht¹, M. M. Fejer⁴⁸, F. Feng²⁷, A. Fernandez-Galiana¹², I. Ferrante^{18,19}, E. C. Ferreira¹³, T. A. Ferreira¹³, F. Ferrini²⁸, F. Fidecaro^{18,19}, I. Fiori²⁸, D. Fiorucci²⁷, M. Fishbach⁸⁹, R. P. Fisher^{41,115}, J. M. Fishner¹², M. Fitz-Axen⁴², R. Flaminio^{32,116}, M. Fletcher⁴³, E. Flynn²⁶, H. Fong¹¹⁷, J. A. Font^{20,118}, P. W. F. Forsyth²¹, J.-D. Fournier⁶⁴, S. Frasca^{31,112}, F. Frasconi¹⁹, Z. Frei¹⁰⁵, A. Freise¹¹, R. Frey⁶⁹, V. Frey²⁵, P. Fritschel¹², V. V. Frolov⁷, P. Fulda⁴⁷, M. Fyffe⁷, H. A. Gabbard⁴³, B. U. Gadre³, S. M. Gaebel¹¹, J. R. Gair¹¹⁹, L. Gammaitoni³⁹, M. R. Ganija⁵⁴, S. G. Gaonkar³, A. Garcia²⁶, C. García-Quirós⁹⁸, F. Garufi^{5,78}, B. Gateley⁴⁴, S. Gaudio³³, G. Gaur¹²⁰, V. Gayathri¹²¹, G. Gemme⁵⁹, E. Genin²⁸, A. Gennai¹⁹, D. George¹⁷, J. George⁶⁰, L. Gergely¹²², V. Germain³², S. Ghonge⁷⁶, Abhirup Ghosh¹⁶, Archisman Ghosh³⁶, S. Ghosh²³, B. Giacomazzo^{95,111}, J. A. Giaime^{2,7}, K. D. Giardino⁷, A. Giazotto^{19,179}, K. Gill³³, G. Giordano^{4,5}, L. Glover¹¹⁰, P. Godwin⁸⁶, E. Goetz⁴⁴, R. Goetz⁴⁷, B. Goncharov⁶, G. González², J. M. Gonzalez Castro^{18,19}, A. Gopakumar¹²³, M. L. Gorodetsky⁶¹, S. E. Gossan¹, M. Gosselin²⁸, R. Gouaty³², A. Grado^{5,124}, C. Graef⁴³, M. Granata²², A. Grant⁴³, S. Gras¹², P. Grassia¹, C. Gray⁴⁴, R. Gray⁴³, G. Greco^{71,72}, A. C. Green^{11,47}, R. Green⁶⁷, E. M. Gretarsson³³, P. Groot⁶³, H. Grote⁶⁷, S. Grunewald³⁵, P. Gruning²⁵, G. M. Guidi^{71,72}, H. K. Gulati¹⁰⁶, Y. Guo³⁶, A. Gupta⁸⁶, M. K. Gupta¹⁰⁶, E. K. Gustafson¹, R. Gustafson¹²⁵, L. Haegel⁹⁸, O. Halim^{14,15}, B. R. Hall⁶⁸, E. D. Hall¹², E. Z. Hamilton⁶⁷, G. Hammond⁴³, M. Haney⁶⁵,

M. M. Hanke^{8,9}, J. Hanks⁴⁴, C. Hanna⁸⁶, O. A. Hannuksela⁹⁰, J. Hanson⁷, T. Hardwick², K. Haris¹⁶, J. Harms^{14,15}, G. M. Harry¹²⁶, I. W. Harry³⁵, C.-J. Haster¹¹⁷, K. Haughian⁴³, F. J. Hayes⁴³, J. Healy⁵⁷, A. Heidmann⁷⁰, M. C. Heintze⁷, H. Heitmann⁶⁴, P. Hello²⁵, G. Hemming²⁸, M. Hendry⁴³, I. S. Heng⁴³, J. Hennig^{8,9}, A. W. Heptonstall¹, Francisco Hernandez Vivanco⁶, M. Heurs^{8,9}, S. Hild⁴³, T. Hinderer^{36,127,128}, D. Hoak²⁸, S. Hochheim^{8,9}, D. Hofman²², A. M. Holgado¹⁷, N. A. Holland²¹, K. Holt⁷, D. E. Holz⁸⁹, P. Hopkins⁶⁷, C. Horst²³, J. Hough⁴³, E. J. Howell⁶², C. G. Hoy⁶⁷, A. Hreibi⁶⁴, E. A. Huerta¹⁷, D. Huet²⁵, B. Hughey³³, M. Hulko¹, S. Husa⁹⁸, S. H. Huttner⁴³, T. Huynh-Dinh⁷, B. Idzkowski⁷³, A. Iess^{29,30}, C. Ingram⁵⁴, R. Inta⁸³, G. Intini^{31,112}, B. Irwin¹¹⁴, H. N. Isa⁴³, J.-M. Isac⁷⁰, M. Isi¹, B. R. Iyer¹⁶, K. Izumi⁴⁴, T. Jacqmin⁷⁰, S. J. Jadhav¹²⁹, K. Jani⁷⁶, N. N. Janthalur¹²⁹, P. Jaranowski¹³⁰, A. C. Jenkins¹³¹, J. Jiang⁴⁷, D. S. Johnson¹⁷, A. W. Jones¹¹, D. I. Jones¹³², R. Jones⁴³, R. J. G. Jonker³⁶, L. Ju⁶², J. Junker^{8,9}, C. V. Kalaghatgi⁶⁷, V. Kalogera⁵⁸, B. Kamai¹, S. Kandhasamy⁸⁴, G. Kang³⁷, J. B. Kanner¹, S. J. Kapadia²³, S. Karki⁶⁹, K. S. Karvinen^{8,9}, R. Kashyap¹⁶, M. Kasprzak¹, S. Katsanevas²⁸, E. Katsavounidis¹², W. Katzman⁷, S. Kaufer⁹, K. Kawabe⁴⁴, N. V. Keerthana³, F. Kéfélian⁶⁴, D. Keitel⁴³, R. Kennedy¹⁰⁷, J. S. Key¹³³, F. Y. Khalili⁶¹, H. Khan²⁶, I. Khan^{14,30}, S. Khan^{8,9}, Z. Khan¹⁰⁶, E. A. Khazanov¹³⁴, M. Khurshed⁶⁰, N. Kijbunchoo²¹, Chunglee Kim¹³⁵, J. C. Kim¹³⁶, K. Kim⁹⁰, W. Kim⁵⁴, W. S. Kim¹³⁷, Y.-M. Kim¹³⁸, C. Kimball⁵⁸, E. J. King⁵⁴, P. J. King⁴⁴, M. Kinley-Hanlon¹²⁶, R. Kirchhoff^{8,9}, J. S. Kissel⁴⁴, L. Kleybolte¹³⁹, J. H. Klika²³, S. Klimenko⁴⁷, T. D. Knowles³⁸, P. Koch^{8,9}, S. M. Koehlenbeck^{8,9}, G. Koekoek^{36,140}, S. Koley³⁶, V. Kondrashov¹, A. Kontos¹², N. Koper^{8,9}, M. Korobko¹³⁹, W. Z. Korth¹, I. Kowalska⁷³, D. B. Kozak¹, V. Kringel^{8,9}, N. Krishnendu¹⁴¹, A. Królak^{142,143}, G. Kuehn^{8,9}, A. Kumar¹²⁹, P. Kumar¹⁴⁴, R. Kumar¹⁰⁶, S. Kumar¹⁶, L. Kuo⁸⁷, A. Kutynia¹⁴², S. Kwang²³, B. D. Lackey³⁵, K. H. Lai⁹⁰, T. L. Lam⁹⁰, M. Landry⁴⁴, B. B. Lane¹², R. N. Lang¹⁴⁵, J. Lange⁵⁷, B. Lantz⁴⁸, R. K. Lanza¹², A. Lartaux-Vollard²⁵, P. D. Lasky⁶, M. Laxen⁷, A. Lazzarini¹, C. Lazzaro⁵¹, P. Leaci^{31,112}, S. Leavey^{8,9}, Y. K. Lecoecue⁴⁴, C. H. Lee⁹², H. K. Lee¹⁴⁶, H. M. Lee¹⁴⁷, H. W. Lee¹³⁶, J. Lee⁹¹, K. Lee⁴³, J. Lehmann^{8,9}, A. Lenon³⁸, N. Leroy²⁵, N. Letendre³², Y. Levin^{6,97}, J. Li⁸², K. J. L. Li⁹⁰, T. G. F. Li⁹⁰, X. Li⁴⁵, F. Lin⁶, F. Linde³⁶, S. D. Linker¹¹⁰, T. B. Littenberg¹⁴⁸, J. Liu⁶², X. Liu²³, R. K. L. Lo^{1,90}, N. A. Lockerbie²⁴, L. T. London⁶⁷, A. Longo^{149,150}, M. Lorenzini^{14,15}, V. Lorette¹⁵¹, M. Lormand⁷, G. Losurdo¹⁹, J. D. Lough^{8,9}, C. O. Lousto⁵⁷, G. Lovelace²⁶, M. E. Lower¹⁵², H. Lück^{8,9}, D. Lumaca^{29,30}, A. P. Lundgren¹⁵³, R. Lynch¹², Y. Ma⁴⁵, R. Macas⁶⁷, S. Macfoy²⁴, M. MacInnis¹², D. M. Macleod⁶⁷, A. Macquet⁶⁴, F. Magaña-Sandoval⁴¹, L. Magaña Zertuche⁸⁴, R. M. Magee⁸⁶, E. Majorana³¹, I. Maksimovic¹⁵¹, A. Malik⁶⁰, N. Man⁶⁴, V. Mandic⁴², V. Mangano⁴³, G. L. Mansell^{12,44}, M. Manske^{21,23}, M. Mantovani²⁸, F. Marchesoni^{40,49}, F. Marion³², S. Márka⁹⁷, Z. Márka⁹⁷, C. Markakis^{10,17}, A. S. Markosyan⁴⁸, A. Markowitz¹, E. Maros¹, A. Marquina¹⁰¹, S. Marsat³⁵, F. Martelli^{71,72}, I. W. Martin⁴³, R. M. Martin³⁴, D. V. Martynov¹¹, K. Mason¹², E. Massera¹⁰⁷, A. Masserot³², T. J. Massinger¹, M. Masso-Reid⁴³, S. Mastrogiovanni^{31,112}, A. Matas^{35,42}, F. Matchard^{1,12}, L. Matone⁹⁷, N. Mavalvala¹², N. Mazumder⁶⁸, J. J. McCann⁶², R. McCarthy⁴⁴, D. E. McClelland²¹, S. McCormick⁷, L. McCuller¹², S. C. McGuire¹⁵⁴, J. McIver¹, D. J. McManus²¹, T. McRae²¹, S. T. McWilliams³⁸, D. Meacher⁸⁶, G. D. Meadors⁶, M. Mehmet^{8,9}, A. K. Mehta¹⁶, J. Meidam³⁶, A. Melatos⁹⁶, G. Mendell⁴⁴, R. A. Mercer²³, L. Mereni²², E. L. Merilh⁴⁴, M. Merzougui⁶⁴, S. Meshkov¹, C. Messenger⁴³, C. Messick⁸⁶, R. Metzdrorf⁷⁰, P. M. Meyers⁹⁶, H. Miao¹¹, C. Michel²², H. Middleton⁹⁶, E. E. Mikhailov¹⁵⁵, L. Milano^{5,78}, A. L. Miller⁴⁷, A. Miller^{31,112}, M. Millhouse⁵², J. C. Mills⁶⁷, M. C. Milovich-Goff¹¹⁰, O. Minazzoli^{64,156}, Y. Minenkov³⁰, A. Mishkin⁴⁷, C. Mishra¹⁵⁷, T. Mistry¹⁰⁷, S. Mitra³, V. P. Mitrofanov⁶¹, G. Mitselmakher⁴⁷, R. Mittleman¹², G. Mo⁹³, D. Moffa¹¹⁴, K. Mogushi⁸⁴, S. R. P. Mohapatra¹², M. Montani^{71,72}, C. J. Moore¹⁰, D. Moraru⁴⁴, G. Moreno⁴⁴, S. Morisaki⁸¹, B. Mours³², C. M. Mow-Lowry¹¹, Arunava Mukherjee^{8,9}, D. Mukherjee²³, S. Mukherjee¹⁰³, N. Mukund³, A. Mullavey⁷, J. Munch⁵⁴, E. A. Muñiz⁴¹, M. Muratore³³, P. G. Murray⁴³, A. Nagar^{85,158,159}, I. Nardecchia^{29,30}, L. Naticchioni^{31,112}, R. K. Nayak¹⁶⁰, J. Neilson¹¹⁰, G. Nelemans^{36,63}, T. J. N. Nelson⁷, M. Nery^{8,9}, A. Neunzert¹²⁵, K. Y. Ng¹², S. Ng⁵⁴, P. Nguyen⁶⁹, D. Nichols^{36,127}, S. Nissanke^{36,127}, A. Nitz⁸, F. Nocera²⁸, C. North⁶⁷, L. K. Nuttall¹⁵³, M. Obergaulinger²⁰, J. Oberling⁴⁴, B. D. O'Brien⁴⁷, G. D. O'Dea¹¹⁰, G. H. Ogil¹⁶¹, J. J. Oh¹³⁷, S. H. Oh¹³⁷, F. Ohme^{8,9}, H. Ohta⁸¹, M. A. Okada¹³, M. Oliver⁹⁸, P. Oppermann^{8,9}, Richard J. Oram⁷, B. O'Reilly⁷, R. G. Ormiston⁴², L. F. Ortega⁴⁷, R. O'Shaughnessy⁵⁷, S. Ossokine³⁵, D. J. Ottaway⁵⁴, H. Overmier⁷, B. J. Owen⁸³, A. E. Pace⁸⁶, G. Pagano^{18,19}, M. A. Page⁶², A. Pai¹²¹, S. A. Pai⁶⁰, J. R. Palamos⁶⁹, O. Palashov¹³⁴, C. Palomba³¹, A. Pal-Singh¹³⁹, Huang-Wei Pan⁸⁷, B. Pang⁴⁵, P. T. H. Pang⁹⁰, C. Pankow⁵⁸, F. Pannarale^{31,112}, B. C. Pant⁶⁰, F. Paoletti¹⁹, A. Paoli²⁸, A. Parida³, W. Parker^{7,154}, D. Pascucci⁴³, A. Pasqualetti²⁸, R. Passaquieti^{18,19}, D. Passuello¹⁹, M. Patil¹⁴³, B. Patricelli^{18,19}, B. L. Pearlstone⁴³, C. Pedersen⁶⁷, M. Pedraza¹, R. Pedurand^{22,162}, A. Pele⁷, S. Penn¹⁶³, C. J. Perez⁴⁴, A. Perreca^{95,111}, H. P. Pfeiffer^{35,117}, M. Phelps^{8,9}, K. S. Phukon³, O. J. Piccinni^{31,112}, M. Pichot⁶⁴, F. Piergiovanni^{71,72}, G. Pillant²⁸, L. Pinard²², M. Pirello⁴⁴, M. Pitkin⁴³, R. Poggiani^{18,19}, D. Y. T. Pong⁹⁰, S. Ponrathnam³, P. Popolizio²⁸, E. K. Porter²⁷, J. Powell¹⁵², A. K. Prajapati¹⁰⁶, J. Prasad³, K. Prasai⁴⁸, R. Prasanna¹²⁹, G. Pratten⁹⁸, T. Prestegard²³, S. Privitera³⁵, G. A. Prodi^{95,111}, L. G. Prokhorov⁶¹, O. Puncken^{8,9}, M. Punturo⁴⁰, P. Puppo³¹, M. Pürner³⁵, H. Qi²³, V. Quetschke¹⁰³, P. J. Quinonez³³, E. A. Quintero¹, R. Quitzow-James⁶⁹, F. J. Raab⁴⁴, H. Radkins⁴⁴, N. Radulescu⁶⁴, P. Raffai¹⁰⁵, S. Raja⁶⁰, C. Rajan⁶⁰, B. Rajbhandari⁸³, M. Rakhmanov¹⁰³, K. E. Ramirez¹⁰³, A. Ramos-Buades⁹⁸, Javed Rana³, K. Rao⁵⁸, P. Rapagnani^{31,112}, V. Raymond⁶⁷, M. Razzano^{18,19}, J. Read²⁶, T. Regimbau³², L. Rei⁵⁹, S. Reid²⁴, D. H. Reitze^{1,47}, W. Ren¹⁷, F. Ricci^{31,112}, C. J. Richardson³³, J. W. Richardson¹, P. M. Ricker¹⁷, K. Riles¹²⁵, M. Rizzo⁵⁸, N. A. Robertson^{1,43}, R. Robie⁴³, F. Robinet²⁵, A. Rocchi³⁰, L. Rolland³², J. G. Rollins¹, V. J. Roma⁶⁹, M. Romanelli⁶⁶, R. Romano^{4,5}, C. L. Romel⁴⁴, J. H. Romie⁷, K. Rose¹¹⁴, D. Rosińska^{53,164}, S. G. Rosofsky¹⁷, M. P. Ross¹⁶⁵, S. Rowan⁴³, A. Rüdiger^{8,9,180}, P. Ruggi²⁸, G. Rutins¹⁶⁶, K. Ryan⁴⁴, S. Sachdev¹, T. Sadecki⁴⁴, M. Sakellariadou¹³¹, L. Salconi²⁸, M. Saleem¹⁴¹, A. Samajdar³⁶, L. Sammut⁶, E. J. Sanchez¹, L. E. Sanchez¹, N. Sanchis-Gual²⁰, V. Sandberg⁴⁴, J. R. Sanders⁴¹, K. A. Santiago³⁴, N. Sarin⁶, B. Sassolas²², P. R. Saulson⁴¹,

O. Sauter¹²⁵, R. L. Savage⁴⁴, P. Schale⁶⁹, M. Scheel⁴⁵, J. Scheuer⁵⁸, P. Schmidt⁶³, R. Schnabel¹³⁹, R. M. S. Schofield⁶⁹, A. Schönbeck¹³⁹, E. Schreiber^{8,9}, B. W. Schulte^{8,9}, B. F. Schutz⁶⁷, S. G. Schwalbe³³, J. Scott⁴³, S. M. Scott²¹, E. Seidel¹⁷, D. Sellers⁷, A. S. Sengupta¹⁶⁷, N. Sennett³⁵, D. Sentenac²⁸, V. Sequino^{14,29,30}, A. Sergeev¹³⁴, Y. Setyawati^{8,9}, D. A. Shaddock²¹, T. Shaffer⁴⁴, M. S. Shahriar⁵⁸, M. B. Shaner¹¹⁰, L. Shao³⁵, P. Sharma⁶⁰, P. Shawhan⁷⁵, H. Shen¹⁷, R. Shink¹⁶⁸, D. H. Shoemaker¹², D. M. Shoemaker⁷⁶, S. ShyamSundar⁶⁰, K. Siellez⁷⁶, M. Sieniawska⁵³, D. Sigg⁴⁴, A. D. Silva¹³, L. P. Singer⁷⁹, N. Singh⁷³, A. Singhal^{14,31}, A. M. Sintes⁹⁸, S. Sitmukhambetov¹⁰³, V. Skliris⁶⁷, B. J. J. Slagmolen²¹, T. J. Slaven-Blair⁶², J. R. Smith²⁶, R. J. E. Smith⁶, S. Somala¹⁶⁹, E. J. Son¹³⁷, B. Sorazu⁴³, F. Sorrentino⁵⁹, T. Souradeep³, E. Sowell⁸³, A. P. Spencer⁴³, A. K. Srivastava¹⁰⁶, V. Srivastava⁴¹, K. Staats⁵⁸, C. Stachie⁶⁴, M. Standke^{8,9}, D. A. Steer²⁷, M. Steinke^{8,9}, J. Steinlechner^{43,139}, S. Steinlechner¹³⁹, D. Steinmeyer^{8,9}, S. P. Stevenson¹⁵², D. Stocks⁴⁸, R. Stone¹⁰³, D. J. Stops¹¹, K. A. Strain⁴³, G. Stratta^{71,72}, S. E. Strigin⁶¹, A. Strunk⁴⁴, R. Sturani¹⁷⁰, A. L. Stuver¹⁷¹, V. Sudhir¹², T. Z. Summerscales¹⁷², L. Sun¹, S. Sunil¹⁰⁶, J. Suresh³, P. J. Sutton⁶⁷, B. L. Swinkels³⁶, M. J. Szczepańczyk³³, M. Tacca³⁶, S. C. Tait⁴³, C. Talbot⁶, D. Talukder⁶⁹, D. B. Tanner⁴⁷, M. Tápai¹²², A. Taracchini³⁵, J. D. Tasson⁹³, R. Taylor¹, F. Thies^{8,9}, M. Thomas⁷, P. Thomas⁴⁴, S. R. Thondapu⁶⁰, K. A. Thorne⁷, E. Thrane⁶, Shubhanshu Tiwari^{95,111}, Srishti Tiwari¹²³, V. Tiwari⁶⁷, K. Toland⁴³, M. Tonelli^{18,19}, Z. Tornasi⁴³, A. Torres-Forné¹⁷³, C. I. Torrie¹, D. Töyrä¹¹, F. Travasso^{28,40}, G. Traylor⁷, M. C. Tringali⁷³, A. Trovato²⁷, L. Trozzo^{19,174}, R. Trudeau¹, K. W. Tsang³⁶, M. Tse¹², R. Tso⁴⁵, L. Tsukada⁸¹, D. Tsuna⁸¹, D. Tuyenbayev¹⁰³, K. Ueno⁸¹, D. Ugolini¹⁷⁵, C. S. Unnikrishnan¹²³, A. L. Urban², S. A. Usman⁶⁷, H. Vahlbruch⁹, G. Vajente¹, G. Valdes², N. van Bakel³⁶, M. van Beuzekom³⁶, J. F. J. van den Brand^{36,74}, C. Van Den Broeck^{36,176}, D. C. Vander-Hyde⁴¹, J. V. van Heijningen⁶², L. van der Schaaf³⁶, A. A. van Veggel⁴³, M. Vardaro^{50,51}, V. Varma⁴⁵, S. Vass¹, M. Vasúth⁴⁶, A. Vecchio¹¹, G. Vedovato⁵¹, J. Veitch⁴³, P. J. Veitch⁵⁴, K. Venkateswara¹⁶⁵, G. Venugopalan¹, D. Verkindt³², F. Vetranò^{71,72}, A. Viceré^{71,72}, A. D. Viets²³, D. J. Vine¹⁶⁶, J.-Y. Vinet⁶⁴, S. Vitale¹², T. Vo⁴¹, H. Vocca^{39,40}, C. Vorvick⁴⁴, S. P. Vyatchanin⁶¹, A. R. Wade¹, L. E. Wade¹¹⁴, M. Wade¹¹⁴, R. Walet³⁶, M. Walker²⁶, L. Wallace¹, S. Walsh²³, G. Wang^{14,19}, H. Wang¹¹, J. Z. Wang¹²⁵, W. H. Wang¹⁰³, Y. F. Wang⁹⁰, R. L. Ward²¹, Z. A. Warden³³, J. Warner⁴⁴, M. Was³², J. Watchi⁹⁹, B. Weaver⁴⁴, L.-W. Wei^{8,9}, M. Weinert^{8,9}, A. J. Weinstein¹, R. Weiss¹², F. Wellmann^{8,9}, L. Wen⁶², E. K. Wessel¹⁷, P. Weßels^{8,9}, J. W. Westhouse³³, K. Wette²¹, J. T. Whelan⁵⁷, B. F. Whiting⁴⁷, C. Whittle¹², D. M. Wilken^{8,9}, D. Williams⁴³, A. R. Williamson^{36,127}, J. L. Willis¹, B. Willke^{8,9}, M. H. Wimmer^{8,9}, W. Winkler^{8,9}, C. C. Wipf¹, H. Wittel^{8,9}, G. Woan⁴³, J. Woehler^{8,9}, J. K. Wofford⁵⁷, J. Worden⁴⁴, J. L. Wright⁴³, D. S. Wu^{8,9}, D. M. Wysocki⁵⁷, L. Xiao¹, H. Yamamoto¹, C. C. Yancey⁷⁵, L. Yang¹¹³, M. J. Yap²¹, M. Yazback⁴⁷, D. W. Yeeles⁶⁷, Hang Yu¹², Haocun Yu¹², S. H. R. Yuen⁹⁰, M. Yvert³², A. K. Zadrożny^{103,142}, M. Zanolin³³, T. Zelenova²⁸, J.-P. Zendri⁵¹, M. Zevin⁵⁸, J. Zhang⁶², L. Zhang¹, T. Zhang⁴³, C. Zhao⁶², M. Zhou⁵⁸, Z. Zhou⁵⁸, A. B. Zimmerman¹⁷⁷, X. J. Zhu⁶, M. E. Zucker^{1,12}, and J. Zweizig¹

¹ LIGO, California Institute of Technology, Pasadena, CA 91125, USA

² Louisiana State University, Baton Rouge, LA 70803, USA

³ Inter-University Centre for Astronomy and Astrophysics, Pune 411007, India

⁴ Università di Salerno, Fisciano, I-84084 Salerno, Italy

⁵ INFN, Sezione di Napoli, Complesso Universitario di Monte S. Angelo, I-80126 Napoli, Italy

⁶ OzGrav, School of Physics & Astronomy, Monash University, Clayton 3800, Victoria, Australia

⁷ LIGO Livingston Observatory, Livingston, LA 70754, USA

⁸ Max Planck Institute for Gravitational Physics (Albert Einstein Institute), D-30167 Hannover, Germany

⁹ Leibniz Universität Hannover, D-30167 Hannover, Germany

¹⁰ University of Cambridge, Cambridge CB2 1TN, UK

¹¹ University of Birmingham, Birmingham B15 2TT, UK

¹² LIGO, Massachusetts Institute of Technology, Cambridge, MA 02139, USA

¹³ Instituto Nacional de Pesquisas Espaciais, 12227-010 São José dos Campos, São Paulo, Brazil

¹⁴ Gran Sasso Science Institute (GSSI), I-67100 L'Aquila, Italy

¹⁵ INFN, Laboratori Nazionali del Gran Sasso, I-67100 Assergi, Italy

¹⁶ International Centre for Theoretical Sciences, Tata Institute of Fundamental Research, Bengaluru 560089, India

¹⁷ NCSA, University of Illinois at Urbana-Champaign, Urbana, IL 61801, USA

¹⁸ Università di Pisa, I-56127 Pisa, Italy

¹⁹ INFN, Sezione di Pisa, I-56127 Pisa, Italy

²⁰ Departamento de Astronomía y Astrofísica, Universitat de València, E-46100 Burjassot, València, Spain

²¹ OzGrav, Australian National University, Canberra, Australian Capital Territory 0200, Australia

²² Laboratoire des Matériaux Avancés (LMA), CNRS/IN2P3, F-69622 Villeurbanne, France

²³ University of Wisconsin-Milwaukee, Milwaukee, WI 53201, USA

²⁴ SUPA, University of Strathclyde, Glasgow G1 1XQ, UK

²⁵ LAL, Univ. Paris-Sud, CNRS/IN2P3, Université Paris-Saclay, F-91898 Orsay, France

²⁶ California State University Fullerton, Fullerton, CA 92831, USA

²⁷ APC, AstroParticule et Cosmologie, Université Paris Diderot, CNRS/IN2P3, CEA/Irfu, Observatoire de Paris, Sorbonne Paris Cité, F-75205 Paris Cedex 13, France

²⁸ European Gravitational Observatory (EGO), I-56021 Cascina, Pisa, Italy

²⁹ Università di Roma Tor Vergata, I-00133 Roma, Italy

³⁰ INFN, Sezione di Roma Tor Vergata, I-00133 Roma, Italy

³¹ INFN, Sezione di Roma, I-00185 Roma, Italy

³² Laboratoire d'Annecy de Physique des Particules (LAPP), Univ. Grenoble Alpes, Université Savoie Mont Blanc, CNRS/IN2P3, F-74941 Annecy, France

³³ Embry-Riddle Aeronautical University, Prescott, AZ 86301, USA

³⁴ Montclair State University, Montclair, NJ 07043, USA

³⁵ Max Planck Institute for Gravitational Physics (Albert Einstein Institute), D-14476 Potsdam-Golm, Germany

³⁶ Nikhef, Science Park 105, 1098 XG Amsterdam, The Netherlands

³⁷ Korea Institute of Science and Technology Information, Daejeon 34141, Republic of Korea

³⁸ West Virginia University, Morgantown, WV 26506, USA

- ³⁹ Università di Perugia, I-06123 Perugia, Italy
⁴⁰ INFN, Sezione di Perugia, I-06123 Perugia, Italy
⁴¹ Syracuse University, Syracuse, NY 13244, USA
⁴² University of Minnesota, Minneapolis, MN 55455, USA
⁴³ SUPA, University of Glasgow, Glasgow G12 8QQ, UK
⁴⁴ LIGO Hanford Observatory, Richland, WA 99352, USA
⁴⁵ Caltech CaRT, Pasadena, CA 91125, USA
⁴⁶ Wigner RCP, RMKI, H-1121 Budapest, Konkoly Thege Miklós út 29-33, Hungary
⁴⁷ University of Florida, Gainesville, FL 32611, USA
⁴⁸ Stanford University, Stanford, CA 94305, USA
⁴⁹ Università di Camerino, Dipartimento di Fisica, I-62032 Camerino, Italy
⁵⁰ Università di Padova, Dipartimento di Fisica e Astronomia, I-35131 Padova, Italy
⁵¹ INFN, Sezione di Padova, I-35131 Padova, Italy
⁵² Montana State University, Bozeman, MT 59717, USA
⁵³ Nicolaus Copernicus Astronomical Center, Polish Academy of Sciences, 00-716, Warsaw, Poland
⁵⁴ OzGrav, University of Adelaide, Adelaide, South Australia 5005, Australia
⁵⁵ Theoretisch-Physikalisches Institut, Friedrich-Schiller-Universität Jena, D-07743 Jena, Germany
⁵⁶ INFN, Sezione di Milano Bicocca, Gruppo Collegato di Parma, I-43124 Parma, Italy
⁵⁷ Rochester Institute of Technology, Rochester, NY 14623, USA
⁵⁸ Center for Interdisciplinary Exploration & Research in Astrophysics (CIERA), Northwestern University, Evanston, IL 60208, USA
⁵⁹ INFN, Sezione di Genova, I-16146 Genova, Italy
⁶⁰ RRCAT, Indore, Madhya Pradesh 452013, India
⁶¹ Faculty of Physics, Lomonosov Moscow State University, Moscow 119991, Russia
⁶² OzGrav, University of Western Australia, Crawley, Western Australia 6009, Australia
⁶³ Department of Astrophysics/IMAPP, Radboud University Nijmegen, P.O. Box 9010, 6500 GL Nijmegen, The Netherlands
⁶⁴ Artemis, Université Côte d’Azur, Observatoire Côte d’Azur, CNRS, CS 34229, F-06304 Nice Cedex 4, France
⁶⁵ Physik-Institut, University of Zurich, Winterthurerstrasse 190, 8057 Zurich, Switzerland
⁶⁶ Univ Rennes, CNRS, Institut FOTON—UMR6082, F-3500 Rennes, France
⁶⁷ Cardiff University, Cardiff CF24 3AA, UK
⁶⁸ Washington State University, Pullman, WA 99164, USA
⁶⁹ University of Oregon, Eugene, OR 97403, USA
⁷⁰ Laboratoire Kastler Brossel, Sorbonne Université, CNRS, ENS-Université PSL, Collège de France, F-75005 Paris, France
⁷¹ Università degli Studi di Urbino “Carlo Bo,” I-61029 Urbino, Italy
⁷² INFN, Sezione di Firenze, I-50019 Sesto Fiorentino, Firenze, Italy
⁷³ Astronomical Observatory Warsaw University, 00-478 Warsaw, Poland
⁷⁴ VU University Amsterdam, 1081 HV Amsterdam, The Netherlands
⁷⁵ University of Maryland, College Park, MD 20742, USA
⁷⁶ School of Physics, Georgia Institute of Technology, Atlanta, GA 30332, USA
⁷⁷ Université Claude Bernard Lyon 1, F-69622 Villeurbanne, France
⁷⁸ Università di Napoli “Federico II,” Complesso Universitario di Monte S. Angelo, I-80126 Napoli, Italy
⁷⁹ NASA Goddard Space Flight Center, Greenbelt, MD 20771, USA
⁸⁰ Dipartimento di Fisica, Università degli Studi di Genova, I-16146 Genova, Italy
⁸¹ RESCEU, University of Tokyo, Tokyo, 113-0033, Japan
⁸² Tsinghua University, Beijing 100084, People’s Republic of China
⁸³ Texas Tech University, Lubbock, TX 79409, USA
⁸⁴ The University of Mississippi, University, MS 38677, USA
⁸⁵ Museo Storico della Fisica e Centro Studi e Ricerche “Enrico Fermi,” I-00184 Roma, Italy
⁸⁶ The Pennsylvania State University, University Park, PA 16802, USA
⁸⁷ National Tsing Hua University, Hsinchu City, 30013 Taiwan, Republic of China
⁸⁸ Charles Sturt University, Wagga Wagga, New South Wales 2678, Australia
⁸⁹ University of Chicago, Chicago, IL 60637, USA
⁹⁰ The Chinese University of Hong Kong, Shatin, NT, Hong Kong
⁹¹ Seoul National University, Seoul 08826, Republic of Korea
⁹² Pusan National University, Busan 46241, Republic of Korea
⁹³ Carleton College, Northfield, MN 55057, USA
⁹⁴ INAF, Osservatorio Astronomico di Padova, I-35122 Padova, Italy
⁹⁵ INFN, Trento Institute for Fundamental Physics and Applications, I-38123 Povo, Trento, Italy
⁹⁶ OzGrav, University of Melbourne, Parkville, Victoria 3010, Australia
⁹⁷ Columbia University, New York, NY 10027, USA
⁹⁸ Universitat de les Illes Balears, IAC3—IEEC, E-07122 Palma de Mallorca, Spain
⁹⁹ Université Libre de Bruxelles, Brussels B-1050, Belgium
¹⁰⁰ Sonoma State University, Rohnert Park, CA 94928, USA
¹⁰¹ Departamento de Matemáticas, Universitat de València, E-46100 Burjassot, València, Spain
¹⁰² University of Rhode Island, Kingston, RI 02881, USA
¹⁰³ The University of Texas Rio Grande Valley, Brownsville, TX 78520, USA
¹⁰⁴ Bellevue College, Bellevue, WA 98007, USA
¹⁰⁵ MTA-ELTE Astrophysics Research Group, Institute of Physics, Eötvös University, Budapest 1117, Hungary
¹⁰⁶ Institute for Plasma Research, Bhat, Gandhinagar 382428, India
¹⁰⁷ The University of Sheffield, Sheffield S10 2TN, UK
¹⁰⁸ IGFAE, Campus Sur, Universidade de Santiago de Compostela, E-15782 Spain
¹⁰⁹ Dipartimento di Scienze Matematiche, Fisiche e Informatiche, Università di Parma, I-43124 Parma, Italy
¹¹⁰ California State University, Los Angeles, 5151 State University Dr, Los Angeles, CA 90032, USA
¹¹¹ Università di Trento, Dipartimento di Fisica, I-38123 Povo, Trento, Italy
¹¹² Università di Roma “La Sapienza,” I-00185 Roma, Italy
¹¹³ Colorado State University, Fort Collins, CO 80523, USA
¹¹⁴ Kenyon College, Gambier, OH 43022, USA

- ¹¹⁵ Christopher Newport University, Newport News, VA 23606, USA
- ¹¹⁶ National Astronomical Observatory of Japan, 2-21-1 Osawa, Mitaka, Tokyo 181-8588, Japan
- ¹¹⁷ Canadian Institute for Theoretical Astrophysics, University of Toronto, Toronto, Ontario M5S 3H8, Canada
- ¹¹⁸ Observatori Astronòmic, Universitat de València, E-46980 Paterna, València, Spain
- ¹¹⁹ School of Mathematics, University of Edinburgh, Edinburgh EH9 3FD, UK
- ¹²⁰ Institute Of Advanced Research, Gandhinagar 382426, India
- ¹²¹ Indian Institute of Technology Bombay, Powai, Mumbai 400 076, India
- ¹²² University of Szeged, Dóm tér 9, Szeged 6720, Hungary
- ¹²³ Tata Institute of Fundamental Research, Mumbai 400005, India
- ¹²⁴ INAF, Osservatorio Astronomico di Capodimonte, I-80131, Napoli, Italy
- ¹²⁵ University of Michigan, Ann Arbor, MI 48109, USA
- ¹²⁶ American University, Washington, DC 20016, USA
- ¹²⁷ GRAPPA, Anton Pannekoek Institute for Astronomy and Institute of High-Energy Physics, University of Amsterdam, Science Park 904, 1098 XH Amsterdam, The Netherlands
- ¹²⁸ Delta Institute for Theoretical Physics, Science Park 904, 1090 GL Amsterdam, The Netherlands
- ¹²⁹ Directorate of Construction, Services & Estate Management, Mumbai 400094, India
- ¹³⁰ University of Białystok, 15-424 Białystok, Poland
- ¹³¹ King's College London, University of London, London WC2R 2LS, UK
- ¹³² University of Southampton, Southampton SO17 1BJ, UK
- ¹³³ University of Washington Bothell, Bothell, WA 98011, USA
- ¹³⁴ Institute of Applied Physics, Nizhny Novgorod, 603950, Russia
- ¹³⁵ Ewha Womans University, Seoul 03760, Republic of Korea
- ¹³⁶ Inje University Gimhae, South Gyeongsang 50834, Republic of Korea
- ¹³⁷ National Institute for Mathematical Sciences, Daejeon 34047, Republic of Korea
- ¹³⁸ Ulsan National Institute of Science and Technology, Ulsan 44919, Republic of Korea
- ¹³⁹ Universität Hamburg, D-22761 Hamburg, Germany
- ¹⁴⁰ Maastricht University, P.O. Box 616, 6200 MD Maastricht, The Netherlands
- ¹⁴¹ Chennai Mathematical Institute, Chennai 603103, India
- ¹⁴² NCBJ, 05-400 Świerk-Otwock, Poland
- ¹⁴³ Institute of Mathematics, Polish Academy of Sciences, 00656 Warsaw, Poland
- ¹⁴⁴ Cornell University, Ithaca, NY 14850, USA
- ¹⁴⁵ Hillsdale College, Hillsdale, MI 49242, USA
- ¹⁴⁶ Hanyang University, Seoul 04763, Republic of Korea
- ¹⁴⁷ Korea Astronomy and Space Science Institute, Daejeon 34055, Republic of Korea
- ¹⁴⁸ NASA Marshall Space Flight Center, Huntsville, AL 35811, USA
- ¹⁴⁹ Dipartimento di Matematica e Fisica, Università degli Studi Roma Tre, I-00146 Roma, Italy
- ¹⁵⁰ INFN, Sezione di Roma Tre, I-00146 Roma, Italy
- ¹⁵¹ ESPCI, CNRS, F-75005 Paris, France
- ¹⁵² OzGrav, Swinburne University of Technology, Hawthorn VIC 3122, Australia
- ¹⁵³ University of Portsmouth, Portsmouth, PO1 3FX, UK
- ¹⁵⁴ Southern University and A&M College, Baton Rouge, LA 70813, USA
- ¹⁵⁵ College of William and Mary, Williamsburg, VA 23187, USA
- ¹⁵⁶ Centre Scientifique de Monaco, 8 quai Antoine 1er, MC-98000, Monaco
- ¹⁵⁷ Indian Institute of Technology Madras, Chennai 600036, India
- ¹⁵⁸ INFN Sezione di Torino, Via P. Giuria 1, I-10125 Torino, Italy
- ¹⁵⁹ Institut des Hautes Etudes Scientifiques, F-91440 Bures-sur-Yvette, France
- ¹⁶⁰ IISER-Kolkata, Mohanpur, West Bengal 741252, India
- ¹⁶¹ Whitman College, 345 Boyer Avenue, Walla Walla, WA 99362 USA
- ¹⁶² Université de Lyon, F-69361 Lyon, France
- ¹⁶³ Hobart and William Smith Colleges, Geneva, NY 14456, USA
- ¹⁶⁴ Janusz Gil Institute of Astronomy, University of Zielona Góra, 65-265 Zielona Góra, Poland
- ¹⁶⁵ University of Washington, Seattle, WA 98195, USA
- ¹⁶⁶ SUPA, University of the West of Scotland, Paisley PA1 2BE, UK
- ¹⁶⁷ Indian Institute of Technology, Gandhinagar Ahmedabad Gujarat 382424, India
- ¹⁶⁸ Université de Montréal/Polytechnique, Montreal, Quebec H3T 1J4, Canada
- ¹⁶⁹ Indian Institute of Technology Hyderabad, Sangareddy, Khandi, Telangana 502285, India
- ¹⁷⁰ International Institute of Physics, Universidade Federal do Rio Grande do Norte, Natal RN 59078-970, Brazil
- ¹⁷¹ Villanova University, 800 Lancaster Ave, Villanova, PA 19085, USA
- ¹⁷² Andrews University, Berrien Springs, MI 49104, USA
- ¹⁷³ Max Planck Institute for Gravitationalphysik (Albert Einstein Institute), D-14476 Potsdam-Golm, Germany
- ¹⁷⁴ Università di Siena, I-53100 Siena, Italy
- ¹⁷⁵ Trinity University, San Antonio, TX 78212, USA
- ¹⁷⁶ Van Swinderen Institute for Particle Physics and Gravity, University of Groningen, Nijenborgh 4, 9747 AG Groningen, The Netherlands
- ¹⁷⁷ Department of Physics, University of Texas, Austin, TX 78712, USA

Received 2019 January 28; revised 2019 February 18; accepted 2019 February 18; published 2019 April 25

¹⁷⁸ Deceased, 2018 February.

¹⁷⁹ Deceased, 2017 November.

¹⁸⁰ Deceased, 2018 July.



Abstract

Advanced LIGO’s second observing run (O2), conducted from 2016 November 30 to 2017 August 25, combined with Advanced Virgo’s first observations in 2017 August, witnessed the birth of gravitational-wave multimessenger astronomy. The first ever gravitational-wave detection from the coalescence of two neutron stars, GW170817, and its gamma-ray counterpart, GRB 170817A, led to an electromagnetic follow-up of the event at an unprecedented scale. Several teams from across the world searched for EM/neutrino counterparts to GW170817, paving the way for the discovery of optical, X-ray, and radio counterparts. In this article, we describe the online identification of gravitational-wave transients and the distribution of gravitational-wave alerts by the LIGO and Virgo collaborations during O2. We also describe the gravitational-wave observables that were sent in the alerts to enable searches for their counterparts. Finally, we give an overview of the online candidate alerts shared with observing partners during O2. Alerts were issued for 14 candidates, 6 of which have been confirmed as gravitational-wave events associated with the merger of black holes or neutron stars. Of the 14 alerts, 8 were issued less than an hour after data acquisition.

Key words: gravitational waves – methods: data analysis

1. Introduction

Gravitational-wave (GW) multimessenger astronomy provides a unique view of the cosmos. In this paper, we explain the procedures used during the second observing run of the advanced ground-based gravitational-wave-detector network to issue alerts for multimessenger follow-up. We also include a summary of all alerts issued to observing partners and an update on the status of candidate events.

The Advanced Laser Interferometer Gravitational-wave Observatory (LIGO) detectors (LIGO Scientific Collaboration et al. 2015) are installed in the US at Hanford, WA and Livingston, LA, and the Advanced Virgo detector (Acernese et al. 2015) is located in Cascina, Italy near Pisa. The detectors use a modified Michelson laser interferometer design to measure GW strain. A passing GW causes a differential length change in the detector arms, producing interference of the laser beams at the beam splitter, and giving an optical readout proportional to the GW strain.

In 2015 September the two Advanced LIGO detectors began their first observing run (O1), lasting four months. The first direct detection of gravitational waves, GW150914, from the coalescence of binary black holes (BBHs; Abbott et al. 2016b), marked the beginning of gravitational-wave (GW) astronomy. Two additional BBH merger signals, GW151012¹⁸¹ (Abbott et al. 2016c) and GW151226 (Abbott et al. 2016d), were identified before the end of O1. Following hardware and software upgrades, the second Advanced LIGO observing run (O2) began on 2016 November 30. Advanced Virgo joined the network in 2017 August for the last month of data acquisition.

A number of additional BBH coalescences were detected in O2 (see Abbott et al. 2017a, 2017b, 2017c, LIGO Scientific Collaboration et al. 2018). Furthermore, on 2017 August 17, at 12:41:04 UTC a binary neutron star (BNS) inspiral signal (GW170817) was observed (Abbott et al. 2017d). Less than two seconds later, the short gamma-ray burst (sGRB) GRB 170817A was detected by two space-based instruments: the Gamma-ray Burst Monitor (GBM) on board *Fermi* (Goldstein et al. 2017), and the spectrometer anti-coincidence shield (SPi-ACS) on board *INTEGRAL* (Savchenko et al. 2017). This joint observation provided the first direct evidence that at least a fraction of sGRBs have a BNS system as a progenitor, as predicted by Eichler et al. (1989), Paczynski (1986), and Paczynski (1991). Short GRBs are typically expected to result

in a long-lasting, multiwavelength afterglow emission in X-ray, optical, and radio bands (for a review see Nakar 2007; Berger 2014; D’Avanzo 2015).

The extensive electromagnetic (EM) observational campaign using the well-constrained, three-detector skymap from the detection of GW170817 led to the discovery of an optical transient (SSS17a/AT 2017gfo) in the host galaxy NGC 4993 (Coulter et al. 2017); the counterpart was also detected at ultraviolet and infrared wavelengths (Abbott et al. 2017e). Photometric and spectroscopic observations of the counterpart support the hypothesis that BNS mergers are sites of r-process nucleosynthesis of heavy elements that decay, thus powering so-called kilonova emission in UV/optical/NIR (see, e.g., Li & Paczyński 1998; Kulkarni 2005; Tanaka 2016; Evans et al. 2017; Kasen et al. 2017; Metzger 2017; Pian et al. 2017; Villar et al. 2017). Several days after the BNS merger, X-ray (Troja et al. 2017) and radio (Hallinan et al. 2017a) emissions were also discovered at the transient’s position (see also Abbott et al. 2017e and references therein). These observations are consistent with the expected interaction of merger ejecta with the interstellar medium on timescales of up to years (see, e.g., Nakar & Piran 2011; Hotokezaka & Piran 2015; Hotokezaka et al. 2016). Data from exhaustive follow-up in the X-ray, radio, and optical, covering almost one year, allowed detailed modeling of emission mechanisms, such as an off-axis structured jet (see, e.g., D’Avanzo et al. 2018; Dobie et al. 2018; Margutti et al. 2018; Mooley et al. 2018a; Ruan et al. 2018). The degeneracy among the various models has been broken with late-time radio observations that support the emergence of a relativistic jet from the BNS merger (Ghirlanda et al. 2018; Mooley et al. 2018b).

Besides compact binary mergers, other transient GW sources that may be observed by ground-based interferometers include the core-collapse of massive stars, which are expected to emit GWs if some asymmetry is present (see Kotake et al. 2006; Ott 2009; Gossan et al. 2016 for an overview). The core-collapse of a massive star is accompanied by supernova (SN) emissions, starting in the ultraviolet and soft X-ray bands from the shock breakout of the stellar surface (see, e.g., Falk & Arnett 1977; Klein & Chevalier 1978; Ensmann & Burrows 1992; Andreoni et al. 2016), and followed by emissions at optical and radio frequencies that typically start from days to weeks after the collapse and last for weeks up to years. Neutrinos are also emitted during core-collapse supernovae as confirmed on 1987 February 23 when MeV neutrinos were detected from SN 1987A in the Large Magellanic Cloud (at a

¹⁸¹ The candidate LVT151012 has been confirmed as a gravitational-wave event, and is now called GW151012 (LIGO Scientific Collaboration et al. 2018).

Table 1
Major Parameters of the O2 Online Search Pipelines Based on Compact Binary Merger Waveform Models

	PyCBC Live	GstLAL	MBTAOnline
Total mass	$2 M_{\odot}$ – $500 M_{\odot}$ ^a	$2 M_{\odot}$ – $150 M_{\odot}$ ^a	$2 M_{\odot}$ – $100 M_{\odot}$
Mass ratio	1–98	1–98	1–99
Minimum component mass	$1 M_{\odot}$	$1 M_{\odot}$	$1 M_{\odot}$
Spin magnitude ($m < 2 M_{\odot}$)	0–0.05	0–0.05	0–0.05
Spin magnitude ($m > 2 M_{\odot}$)	0–0.998	0–0.999	0–0.9899
Single-detector S/N threshold for triggering	5.5	4 ^b	5.5 ^c

Notes.

^a The maximum total mass for PyCBC Live and GstLAL is in fact a function of mass ratio and component spins (Dal Canton & Harry 2017; Mukherjee et al. 2018) and we indicate the highest total mass limit over all mass ratios and spins. The offline GstLAL search uses a template bank extended to a larger maximum total mass of $400 M_{\odot}$.

^b This threshold was applied to the two LIGO detectors only for the online GstLAL analysis. The minimum trigger S/N in Virgo was not determined by an explicit threshold, but instead by a restriction to record at most 1 trigger per second in a given template.

^c MBTAOnline uses a higher LIGO S/N threshold (6) to form coincidences with Virgo.

distance of ~ 50 kpc) by the Kamiokande-II (Hirata et al. 1987) and the Irvine–Michigan–Brookhaven (Bionta et al. 1987) neutrino detectors, a few hours before its optical counterpart was discovered. In addition, GRBs and SNe are expected to produce relativistic outflows in which particles (protons and nuclei) can be accelerated and produce high-energy neutrinos by interacting with the surrounding medium and radiation (see, e.g., Murase 2018).

Another class of transient GW sources is magnetars, i.e., rotating NSs with very intense magnetic fields ($\sim 10^{15}$ G). Theoretical models predict that when these stars undergo starquakes, asymmetric strains can temporarily alter the geometry of the star and GWs can be emitted (see, e.g., Corsi & Owen 2011). Electromagnetic phenomena possibly associated with magnetar starquakes include soft gamma repeaters (SGRs) and anomalous X-ray pulsars (AXPs), sources that sporadically emit short bursts of gamma-rays and X-rays (see Mereghetti 2008 for a review). Starquakes can also cause radio/X-ray pulsar glitches: sudden increases in the rotational frequency of a highly magnetized, rotating NS (pulsar) followed by exponential decays, which bring the pulsar rotational frequency back down to its initial value (see, e.g., Espinoza et al. 2011).

During O1 and O2, extensive EM observing campaigns searched for counterparts to GW candidates identified in low-latency. Significant improvements were made between these two observing runs regarding the data analysis software and source modeling, allowing important additional information to be distributed in low-latency during O2. For CBC events, 3D sky localization maps were released, providing information about the direction and the luminosity distance of the source (Singer et al. 2016a), while in O1, only 2D sky localization maps were provided, without distance information. During O2, probabilities that at least one low-mass object was present in

the coalescing binary system and that tidally disrupted material formed a massive accretion disk around the merged object were reported. This information is useful for assessing the likelihood that a merger could power an EM transient (Foucart 2012; Pannarale & Ohme 2014).

During O1 and the first part of O2, with the GW network formed only by the two Advanced LIGO interferometers, sources were typically localized in sky areas ranging from a few hundreds to several thousands of square degrees (see, e.g., Abbott et al. 2017a, 2016d, 2016e). Improvements in localization areas have been made since Advanced Virgo joined the gravitational-wave detector network starting 2017 August 1. For instance, GW170814 and GW170817 were localized by the three-detector network within a few tens of square degrees; see Abbott et al. (2017b, 2017d).

Jointly observing the same event in both gravitational waves and electromagnetic radiation provides complementary insights into the progenitor and its local environment. The GW signal is key to determining several physical properties of the source such as the masses and system properties (inclination, orientation, spin, etc.). The EM counterpart provides information about radioactive decay, shocks, the emission mechanism of the central engine, magnetic fields, and beaming; and also probes the surrounding environment of the source (see, for instance, Berger 2014). The detection of an EM counterpart also can give precise localization and lead to the identification of the host galaxy of the source. The distance estimated from the GW data, combined with the measured redshift of the host galaxy, enables measurement of the Hubble constant (Schutz 1986; Holz & Hughes 2005; Nissanke et al. 2010, 2013a; Abbott et al. 2017f; Hotokezaka et al. 2018; Seto & Kyutoku 2018; Vitale & Chen 2018). Precise measurements of the host galaxy distance and the binary inclination given by the EM observations can be used to reduce the degeneracy in the GW parameter estimation (see, e.g., Guidorzi et al. 2017; Cantiello et al. 2018; Chen et al. 2018; Mandel 2018). Furthermore, the detection of an EM counterpart may increase the confidence in the astrophysical origin of a weak GW signal (Kochanek & Piran 1993). It also provides constraints on the relative merger rates of the two classes of compact binaries (BNS and NS–BH), on the beaming angle of sGRBs, and the NS equation of state (Abadie et al. 2010; Chen & Holz 2013; Pannarale & Ohme 2014; Clark et al. 2015; Dominik et al. 2015; Regimbau et al. 2015; Siellez et al. 2016; Radice et al. 2018). Finally, joint GW and EM observations can provide constraints on fundamental physics (Abbott et al. 2017g).

In this paper, we describe the identification of GW transients and the distribution of GW alerts performed during O2 by the LIGO and Virgo collaborations. We also detail the GW event information shared with the astronomy community and give an overview of the EM follow-up strategies.

In Section 2 we present an overview of the online GW analysis, with a description of the online analysis detection pipelines, and the vetting and approval processes for potential GW events. In Section 3 we summarize the GW alerts that were distributed during O2 and the properties of the gravitational-wave candidates after the offline analysis. We describe the information that was shared with astronomers, including how this was used during the electromagnetic/neutrino follow-up activities. Finally, in Section 4 we present our conclusions.

2. Online Gravitational-wave Analysis

In this section, we describe the two classes of searches for GW transients, modeled and unmodeled, that contributed triggers for low-latency EM follow-up (in Section 2.1). We also present the full vetting and validation process of candidate events (in Section 2.2) and distribution of low-latency alerts during O2 (in Section 2.3). Offline search pipelines¹⁸² also led to the identification of additional candidate events GW170729 and GW170818 (see LIGO Scientific Collaboration et al. 2018).

2.1. Brief Description of Online Pipelines

The modeled (CBC) searches specifically look for signals from compact binary mergers of neutron stars and black holes (BNS, NS–BH, and BBH systems). The unmodeled (burst) searches, on the other hand, are capable of detecting signals from a wide variety of astrophysical sources in addition to compact binary mergers: core-collapse of massive stars, magnetar starquakes, and more speculative sources such as intersecting cosmic strings or currently unknown GW sources.

2.1.1. Online Modeled Searches

GstLAL (Messick et al. 2017), MBTAOnline (Multi-Band Template Analysis, Adams et al. 2016) and PyCBC Live (Nitz et al. 2018) are analysis pipelines designed to detect and report compact binary merger events with sub-minute latencies. Such pipelines use discrete banks of waveform templates to cover the target parameter space of compact binaries and perform matched filtering on the data using those templates, similar to the offline analyses (Usman et al. 2016; Messick et al. 2017) that produced the O1 and O2 catalog of compact binaries (LIGO Scientific Collaboration et al. 2018). The online and offline analyses differ in various ways. The most important configuration choices of online analyses are reviewed here.

The mass and spin parameter space considered by the online pipelines in O2 is summarized in Table 1. All pipelines assume that, while the gravitational-wave signal dwells in the detector sensitive band, the spins of the compact objects are aligned or antialigned with the orbital angular momentum, and that orbital eccentricity is negligible. Additional details of the PyCBC Live and GstLAL banks can be found in Dal Canton & Harry (2017) and Mukherjee et al. (2018), respectively. In the case of PyCBC Live, the online and final offline analyses covered exactly the same space. For GstLAL, the offline bank extended to a larger total mass of $400 M_{\odot}$.

A matched-filtering analysis is performed by each pipeline, producing triggers for each detector’s data stream whenever the matched-filter single-detector signal-to-noise ratio (S/N) peaks above a threshold given in Table 1. Due to the small probability of a signal being detectable in Virgo and not in LIGO during O2, PyCBC Live did not use Virgo to produce triggers; Virgo’s data were nevertheless still analyzed and used for the sky localization of candidates from LIGO.

Matched filtering alone is insufficient in non-Gaussian detector noise, producing frequent non-astrophysical triggers with large S/N (Abbott et al. 2016f). Pipelines can choose among different techniques to mitigate this effect: calculating additional statistics based on the template waveform (signal-

based vetoes), explicitly zeroing out loud and short instrumental transients before matched-filtering (gating), and vetoing triggers based on known data quality issues that are reported with the same latency as the strain data itself. In O2, all matched-filter searches employed signal-based vetoes; PyCBC Live and MBTAOnline applied vetoes based on low-latency data quality information, while GstLAL applied gating.

The trigger lists produced by matched filtering and cleaned via the aforementioned procedures are searched for coincidences between detectors. Coincident triggers are ranked based on their S/Ns and signal-based vetoes and the consistency of their S/Ns, arrival times, and arrival phases at the different detectors with an astrophysical signal. The pipelines construct this ranking and convert it to a statistical significance in different ways, described next. A measure of significance produced by all pipelines for each candidate is the estimated false-alarm rate (FAR), i.e., the rate at which we expect events with at least as high a ranking as the candidate to be generated due to detector noise.

MBTAOnline constructs a background distribution of the ranking statistic by generating every possible coincidence from single-detector triggers over a few hours of recent data. It then folds in the probability of a pair of triggers passing the time coincidence test.

PyCBC Live’s ranking of coincident triggers in O2 was somewhat simpler than the final offline analysis: it did not account for the variation of background over the parameter space (Nitz et al. 2017) and it did not include the sine-Gaussian signal-based veto (Nitz 2018). PyCBC Live estimated the background of accidental coincidences using time shifts between triggers from different detectors, as done by the offline analysis (Usman et al. 2016). The amount of live time used for background estimation in PyCBC Live was 5 hr, to be compared with ~ 5 days of the offline analysis. This choice limited the inverse FAR of online detections to ~ 100 yr maximum, insufficient for claiming a very significant detection, but adequate for generating rapid alerts for astronomers. On the other hand, this choice gave the background estimation a faster response to variations in noise characteristics, which is useful considering the limited data quality flags available to the online analysis.

GstLAL calculates the significance of triggers by constructing a likelihood-ratio ranking statistic that models the distribution of trigger properties for noise and GW events (Cannon et al. 2015). The background is computed by synthesizing likelihood ratios from a random sampling of a probability density that is estimated using non-coincident triggers accumulated over the course of an observing run, which are taken to be noise.

2.1.2. Online Unmodeled Searches

The two unmodeled signal searches (burst), cWB and oLIB, work by looking for excess power in the time-frequency (TF) domain of the GW strain data (Klimenko et al. 2016; Lynch et al. 2017). The cWB pipeline does this by creating TF maps at multiple resolutions across the GW detector network and identifying clusters of TF data samples with power above the baseline detector noise. Excess power clusters in different detectors that overlap in time and frequency indicate the presence of a GW event. The signal waveforms and the source sky location are reconstructed with the maximum likelihood method by maximizing over all possible time-of-flight delays in

¹⁸² The offline O2 results were obtained after a complete regeneration of O2 strain data with noise subtraction performed for the LIGO detectors (Davis et al. 2018).

the detector network. The cWB detection statistic is based on the coherent energy obtained by cross-correlating the signal waveforms reconstructed in the detectors. It is compared to the corresponding background distribution to identify significant GW candidates.

oLIB uses the Q transform to decompose GW strain data into several TF planes of constant quality factors Q , where $Q \sim \tau f_0$. Here, τ and f_0 are the time resolution and central frequency of the transform's filter/wavelet, respectively. The pipeline flags data segments containing excess power and searches for clusters of these segments with identical f_0 and Q spaced within 100 ms of each other. Coincidences among the detector network of clusters with a time-of-flight window up to 10 ms are then analyzed with a coherent (i.e., correlated across the detector network) signal model to identify possible GW candidate events.

Similar to PyCBC Live, both cWB and oLIB use local time slides to estimate the background and calculate the candidates' false-alarm rates (FARs are detailed in Section 3.3.1).

2.2. Vetting and Approval Process

During O1 and O2, all CBC and burst GW triggers were stored in an interactive database (see Section 2.2.1) and required to pass a series of vetting procedures, both automatic (Section 2.2.3) and manual (Section 2.2.4), with the help of supervised protocols (2.2.2).

2.2.1. GraceDb and LVAAlert

The Gravitational-wave Candidate Event Database (GraceDb¹⁸³) is a centralized hub for aggregating and disseminating information about candidate events from GW searches. It features a web interface for displaying event information in a human-friendly format, as well as a representational state transfer application program interface (RESTful API) for programmatic interaction with the service. A Python-based client code package is also maintained to facilitate interactions with the API; this set of tools allows users to add new candidate events to the database, annotate existing events, search for events, upload files, and more.

During O2, GraceDb sent push notifications about candidate event creation and annotation to registered listeners via the LIGO/Virgo Alert System (LVAAlert), a real-time messaging service based on the Extensible Messaging and Presence Protocol (XMPP) and its publish-subscribe (pubsub) extension. Python-based command-line tools were provided to send and receive notifications, create messaging nodes, and manage node subscriptions. Typical receivers of LVAAlert messages were automated follow-up processes that, when triggered, performed tasks such as parameter estimation or detector characterization for a candidate event (details in Section 2.2.3).

2.2.2. Supervised Follow-up Process

Several follow-up processes responded to the entry of a GW candidate into GraceDb, notified by the arrival of an LVAAlert message. Three of these processes were of immediate relevance to the EM follow-up effort: the low-latency sky localization probability map (skymap) generator for CBC triggers, BAYESTAR (Singer & Price 2016), the tracker of candidate event status/incoming information and alert generator/sender

(*approval_processorMP*), and the tracker of other follow-up processing (*eventSupervisor*).

In particular, *approval_processorMP* was responsible for the decision to send alerts based on the following incoming state information: basic trigger properties from the pipelines (FAR, event time, detectors involved with the trigger), data quality and data products (Sections 2.2.3 and 3.3.2), detector operator and advocate signoffs determining the result of human vetting (Section 2.2.4), and other labels identifying time-correlated external triggers or signal injections performed in hardware at the sites. Hardware signal injections are simulated GW signals created by physically displacing the detectors' test masses (Biwer et al. 2017). Triggers with FARs below an agreed-upon FAR threshold and with no injection or data quality veto labels generated alerts to the astronomers involved in the LIGO and Virgo EM follow-up community via the GCN network (see Section 3.2) and GraceDb web services.

2.2.3. Online Automatic Data Vetting

State information was provided to low-latency analysis pipelines indicating when the detectors' data were suitable for use in astrophysical analysis. This included times when the detectors were operating in a nominal state and data calibration was accurate. The low-latency pipelines also dealt with the additional challenge of transient noise artifacts known as glitches, which often occurred in the detectors' data (Abbott et al. 2016f, 2019).

To reduce the effect of glitches, which can mimic true GW signals to some degree but are uncorrelated in the GW detectors, multiple strategies were employed by LIGO and Virgo, including automatically produced data quality vetoes and human vetting of candidate events (see Section 2.2.4). Data quality vetoes indicated times when a noise source known to contaminate the astrophysical searches was active. These vetoes were defined using sensors that measured the behavior of the instruments and their environment. This data quality information was applied in several steps. A set of data quality vetoes was generated in real time and provided to the low-latency pipelines alongside the detector state information. If a candidate GW event occurred during a time that had been vetoed, it was not reported for EM follow-up. Given that these vetoes could potentially prevent a true GW signal from being distributed, this category of data quality information was reserved for severe noise sources.

In parallel with this effort, low-latency algorithms searched LIGO data for correlations between witness sensors and the GW strain data to identify noise sources that might not have been included in defined data quality vetoes. For example, iDQ (a streaming machine learning pipeline based on Essick et al. 2013 and Biswas et al. 2013) reported the probability that there was a glitch in $h(t)$ based on the presence of glitches in witness sensors at the time of the event. In O2, iDQ was used to vet unmodeled low-latency pipeline triggers automatically.

2.2.4. Human Vetting

Human vetting of GW triggers was a critical part of the EM follow-up program, and had to be completed before sending any alert to the astronomers during O2. Potentially interesting triggers were labeled by *approval_processorMP* to require signoffs from follow-up advocates and operators at each relevant detector site.

¹⁸³ <https://gracedb.ligo.org>

Table 2
Characteristics of the Distributed Triggers That Passed the EM Follow-up Validation Process

GW ID	Event Time UTC	Final Status	Source Classification	Triggers		Latency (minutes)	
				Search(es) ^a	Online FAR (yr ⁻¹)	GraceDb submission	Initial GCN Notice
G268556 GW170104 G270580	2017 Jan 04 10:11:58	Confident	BBH EM-Bright: 0%	PyCBC , cWB GstLAL, oLIB	1.9 ^b	264	395
G274296	2017 Jan 20 12:30:59	Retracted	Burst EM-Bright: N/A	cWB	5.0	2	67
G275404	2017 Feb 17 06:05:53	NFI	Burst EM-Bright: N/A	cWB	5.4	715	813
G275697	2017 Feb 25 18:30:21	NFI	NS–BH EM-Bright: 90%	PyCBC , GstLAL	6.0	<1	24
G277583	2017 Feb 27 18:57:31	NFI	BNS EM-Bright: 100%	PyCBC , GstLAL, MBTAOnline	4.5	<1	27
G284239	2017 Mar 13 22:40:09	NFI	Burst EM-Bright: N/A	cWB	2.7	3	30
G288732 GW170608	2017 May 02 22:26:07	NFI	Burst EM-Bright: N/A	oLIB	4.0	12	963
G296853 GW170809	2017 Jun 08 02:01:16	Confident	BBH EM-Bright: 0%	PyCBC , cWB, GstLAL ^c	2.6 ^b	650	818
G297595 GW170814	2017 Aug 09 08:28:22	Confident	BBH EM-Bright: 0%	GstLAL , cWB MBTAOnline	0.2	<1	49
G298048 GW170817	2017 Aug 14 10:30:44	Confident	BBH EM-Bright: 0%	GstLAL , oLIB, PyCBC, cWB ^d	1.2×10^{-5}	<1	31
G298389	2017 Aug 17 12:41:04	Confident	BNS EM-Bright: 100%	GstLAL^d , PyCBC	1.1×10^{-4}	6	27 ^e
G298936 GW170823	2017 Aug 19 15:50:46	NFI	Burst EM-Bright: N/A	oLIB	4.9	16	192
G299232	2017 Aug 23 13:13:59	Confident	BBH EM-Bright: 0%	cWB, oLIB, GstLAL , PyCBC, MBTAOnline	5.5×10^{-4}	<1	22
	2017 Aug 25 13:13:37	NFI	NS–BH EM-Bright: 100%	MBTAOnline^f	5.3	<1	25

Notes. The table provides the following information: time of the GW candidate event, status of the event after offline analysis (confident, i.e., confidently detected GW event; retracted due to further noise investigation; or NFI i.e., no further interest, not present in the offline analysis or consistent with noise), nature of the candidate with an EM-bright classifier (described in Section 3.3.2; if N/A, classifier not available for burst triggers), list of online searches that detected the candidate event (the pipeline selected for the distributed alert is in bold; some of the pipelines are not indicated in the first GCN Circular because they reported the trigger with larger latency), its FAR (online pipeline-dependent, see Section 3.3.1), the latency between the event time and event submission into GraceDb and the delay between the event time and the alert distribution (first GW notice sent to GCN for distribution to partners; see Section 3.2).

^a In bold is the selected pipeline for distribution of the alert to O2 partners.

^b Due to the non-standard way in which this trigger was found, the PyCBC Live low-latency pipeline was run by hand over a short period of data (tens of minutes) in order to produce a trigger for follow-up as quickly as possible. The precision of the FAR estimate is limited by the use of a shorter than normal period of data.

^c The online GstLAL trigger was identified as a single-detector trigger.

^d The sky localization sent to partners five hours after the trigger time was derived from a PyCBC analysis after the high-amplitude glitch in LIGO-Livingston was windowed out (LIGO Scientific Collaboration & Virgo Collaboration 2017b; Abbott et al. 2017d). The FAR was calculated with H1 only.

^e The first circular sent to partners for G298048 informed that a GW candidate event with a single instrument was associated with the time of a Fermi GBM trigger (LIGO Scientific Collaboration & Virgo Collaboration 2017c). The initial Notice sent to partners, at 13:08 UTC, contained a skymap simply representing the quadrupolar antenna response function of the LIGO-Hanford detector over the entire sky.

^f The sky localization sent to partners was derived from a PyCBC analysis (LIGO Scientific Collaboration & Virgo Collaboration 2017d).

Different groups of persons from the collaborations were involved in the decision-making process, including Rapid Response Teams (RRT) with commissioning, computing, and calibration experts from each of the detector sites, pipeline experts, detector characterization experts, and EM follow-up advocates.

First, the on-site operators had to check the status of the instruments within one minute of the trigger, to ensure that unusual events (thunderstorms, trucks driving close to the buildings, etc.) did not happen at the time of the GW trigger and that the interferometer status was nominal.

Second, the experts and on-duty advocates met during an on-call validation process organized immediately after being notified of the trigger. All previously mentioned algorithms in Section 2.2.3 and additional data quality information not accessible at low-latency timescales were considered. For example, the Omega scan and Omicron scan algorithms (Chatterji et al. 2004; Robinet 2016) created time-frequency visualizations of witness sensor data around the time of the candidate event. This allowed for detailed views of instrumental or environmental noise that could potentially influence the detectors' GW strain data. In O2, this information was used to identify false triggers due to noise and veto them before they were reported for EM follow-up.

Third, pipeline experts were asked to check pipeline results, in particular to evaluate the significance of marginal triggers. In the case of more than one viable candidate event (within 1 s for CBC and 5 s for burst triggers), the advocates selected the most promising candidate based on pre-established criteria (e.g., lowest FAR, choosing CBC over burst triggers).

When Virgo joined the LIGO network, it was not used to estimate the FAR of the GW candidate, but only to constrain the sky localization.

Finally, the EM follow-up advocates selected the skymap to send depending on the cross-checks done by the RRT at the different instrument sites, with priority given to the two LIGO detectors as the most sensitive instruments in the network. Then, they released the skymap to the external community and composed the GCN circular (see Section 3.2).

When necessary, the pipeline experts and the data quality team, with the help of the RRT, recommended a retraction after days or weeks, using extended data investigation (Abbott et al. 2019) and/or updated FAR calculation based on additional background data.

2.3. Triggers Distributed during O2

During O2, only GW candidates that passed the above series of checks were distributed to partner astronomers (see Table 2). Approximately half the triggers were rejected during the human vetting process (described in Section 2.2.4) due to the presence of glitches (see Abbott et al. 2018a, 2019). The number of vetoed triggers decreased by 80% from the first half of the O2 observing run to the second due to pipeline software upgrades to avoid transient noise. Other candidate events were vetoed because they were generated due to specific hardware problems or by not meeting the requirements of the O2 alert distribution policy (e.g., single-detector triggers, FAR being above the O2 threshold value, and very high latencies).

A list of distributed triggers during O2 and their online characteristics is provided in Table 2. We note that both CBC and burst pipelines identified the loudest GW candidate events. Six low-latency CBC candidates were ultimately confirmed as GW detections and are described in detail in Abbott et al. (2018a).

G288732 (subsequently named GW170608) occurred when LIGO-Hanford was undergoing angle-to-length decoupling (a regular maintenance procedure that minimizes the coupling between the angular position of the test-mass mirrors and the measurement of the strain) Abbott et al. (2017a), whereas for G268556 (i.e., GW170104), the calibration state was not nominal (Abbott et al. 2017c), creating a high latency in the distribution of alerts. These two real events were recovered due to expert vigilance rather than automated procedures. Moreover, G298048 (i.e., GW170817) was first identified as a single-detector trigger in the LIGO-Hanford data; a glitch in LIGO-Livingston caused the trigger to be rejected and the S/N was too low in Virgo to be detected.

Burst event G270580 was retracted offline due to its correlation with seismic noise (LIGO Scientific Collaboration & Virgo Collaboration 2017a). The CBC candidates G275697, G275404 and G299232 were not present in the offline pipeline analysis, whereas other marginal candidates were listed in LIGO Scientific Collaboration et al. (2018). The burst triggers G274296, G277583, G284239, and G298389 are consistent with background noise based on their event parameters and FARs; hence they are of no further interest. The high latency in sending alerts for the two oLIB events, G284239 and G298389, was due to their skymap generation.

3. Distribution of Alerts

In this section, we present GW candidate information that we distributed and detail how this supported the EM observational campaigns.

3.1. O2 Partners Network

For O2, LIGO/Virgo signed 95 memoranda of understanding (MoUs) with different institutions, agencies, and groups of astronomers from more than 20 countries. The goal was to enable multimessenger observations of astrophysical events by GW detectors with a wide range of telescopes and instruments from EM and neutrino astronomy.

During O2, 88 groups had operational facilities and the ability to receive and send notifications regarding their observations through the GCN network (see Section 3.2). More than 100 space and ground-based instruments were involved in the EM follow-up campaign by covering radio, optical, near-infrared, X-ray, and gamma-ray wavelengths. The telescopes sensitive in the optical bands were the most numerous, representing half of the instruments. The follow-up network also included three facilities capable of detecting high-energy neutrinos: IceCube, ANTARES, Pierre Auger, searching for transients in the northern and southern hemispheres.

3.2. Distribution of the Alerts via the GCN Network

The Gamma-ray Coordinates Network (GCN)¹⁸⁴ was adopted from the GRB community to be used as an alert platform for both LIGO/Virgo observations and multimessenger follow-up. There are two types of GCN alerts: notices and circulars. During O2, the LIGO/Virgo GCN network was private; a requester had to be a member of the LV-EM Forum¹⁸⁵ to receive and send any messages. This is in contrast with normal public operation of GCN as used by the GRB

¹⁸⁴ <https://gcn.gsfc.nasa.gov>

¹⁸⁵ <https://gw-astronomy.org/>

Table 3
Properties of the GW Alerts, Including the Network S/N, the Candidate Event FAR, the Sky Localization Area, and Luminosity Distances

GW ID		Interferometers		S/N ^b	FAR ^b (yr ⁻¹)	Luminosity Distance Median \pm 90% c.i. (Mpc)	Sky Localization Area 50%/90% c.i. (deg ²)	References
		Triggering	Skymap (algorithm)					
G268556	online	H1, L1	H1, L1 (BAYESTAR)	12.4	1.9	730 ⁺³⁴⁰ ₋₃₂₀	430/1630	A
GW170104	offline		H1, L1 (LALInference)	13.0	$<1.4 \times 10^{-5}$	960 ⁺⁴⁴⁰ ₋₄₂₀	200/920	B
G270580	online	H1, L1	H1, L1 (LIB)	8.7	5.0	...	600/3120	C
	offline			D
G274296	online	H1, L1	H1, L1 (cWB)	11.0	5.4	...	430/2140	E
	offline			F
G275404	online	H1, L1	H1, L1 (BAYESTAR)	8.7	6.0	270 ⁺¹⁵⁰ ₋₁₃₀	460/2100	G
	offline	... ^c	H
G275697	online	H1, L1	H1, L1 (BAYESTAR)	8.7	4.5	180 ⁺⁹⁰ ₋₉₀	480/1820	I
	offline	... ^c	J
G277583	online	H1, L1	H1, L1 (cWB, LIB) ^d	9.3	2.7	...	2130/12140 ^d	K
	offline		
G284239	online	H1, L1	H1, L1 (LIB)	8.2	4.0	...	1030/3590	L
	offline		
G288732	online	H1, L1	H1, L1 (BAYESTAR)	12.7	2.6	310 ⁺²⁰⁰ ₋₁₂₀	230/860	M
GW170608	offline		H1, L1 (LALInference)	15.4	$<3.1 \times 10^{-4}$	320 ⁺¹³⁰ ₋₁₀₀	100/400	B
G296853	online	H1, L1	H1, L1 (BAYESTAR)	11.3	0.2	1080 ⁺⁵²⁰ ₋₄₇₀	320/1160	N
GW170809	offline	H1, L1	H1, L1, V1 (LALInference)	12.4	$<1.0 \times 10^{-7}$	980 ⁺³⁵⁰ ₋₃₅₀	70/310 ^e	B
G297595	online	H1, L1	H1, L1, V1 (BAYESTAR)	16.1	1.2×10^{-5}	480 ⁺¹⁹⁰ ₋₁₇₀	22/97 ^e	O
GW170814	offline		H1, L1, V1 (LALInference)	15.9	$<1.0 \times 10^{-7}$	570 ⁺¹⁹⁰ ₋₁₈₀	16/87 ^e	B
G298048	online	H1	H1 (BAYESTAR)	14.5	1.1×10^{-4}	40 ⁺²⁰ ₋₂₀	8060/24220	P
		H1, L1	H1, L1, V1 (BAYESTAR)	40 ⁺¹⁰ ₋₁₀	9/31 ^e	Q
GW170817	offline	H1, L1	H1, L1, V1 (LALInference)	33.0	$<1.0 \times 10^{-7}$	40 ⁺¹⁰ ₋₁₀	5/16 ^e	B
G298389	online	H1, L1	H1, L1 (LIB)	15.6	4.9	...	250/800	R
	offline		
G298936	online	H1, L1	H1, L1 (BAYESTAR)	11.3	5.5×10^{-4}	1380 ⁺⁷⁰⁰ ₋₆₇₀	610/2140	S
		H1, L1	H1, L1, V1 (BAYESTAR)	1540 ⁺⁶⁹⁰ ₋₆₈₀	277/1219 ^e	T
GW170823	offline	H1, L1	H1, L1 (LALInference)	11.5	$<1.0 \times 10^{-7}$	1860 ⁺⁹²⁰ ₋₈₅₀	440/1670	B
G299232	online	H1, L1	H1, L1, V1 (BAYESTAR)	9.1	5.3	330 ⁺²⁰⁰ ₋₁₆₀	451/2040 ^e	U
	offline	... ^c

Notes. Note that sky localization area and luminosity distances for the online search can differ from results mentioned in the distributed GCNs^a. Furthermore, the distance estimates stated in GCN circulars are the a posteriori mean \pm standard deviation, while the distance estimates and confidence intervals stated in the table are the a posteriori median and central 90% intervals. For confident GW events, the table shows results obtained from the offline refined analysis for comparison. Network S/N and FAR are the offline analysis results obtained with the pipeline selected for online distribution of the alerts (see Tables 1 and 2 in LIGO Scientific Collaboration et al. 2018). Offline luminosity distance and sky localization area (50% and 90% confidence regions) are listed also in Table 8 from LIGO Scientific Collaboration et al. (2018), with small differences arising from using the posterior data samples directly versus the generated skymap files.

^a Differences with respect to areas reported in GCN circulars are due to the rounding algorithm used to calculate the enclosed probability of 50% and 90%, which now is more accurate.

^b The network S/N and the false-alarm rate depend on the pipeline that triggered the event.

^c No candidate event was found during the offline analysis.

^d Localization is obtained as the arithmetic mean of cWB and LIB.

^e All skymaps, excluding those using Virgo data, round sky localization areas to the nearest 10; otherwise, they are rounded to the nearest 1.

References. (A) LIGO Scientific Collaboration & Virgo Collaboration (2017e), (B) LIGO Scientific Collaboration et al. (2018), (C) LIGO Scientific Collaboration & Virgo Collaboration (2017f), (D) LIGO Scientific Collaboration & Virgo Collaboration (2017a, 2017g), (E) LIGO Scientific Collaboration & Virgo Collaboration (2017h), (F) LIGO Scientific Collaboration & Virgo Collaboration (2017i), (G) LIGO Scientific Collaboration & Virgo Collaboration (2017j), (H) LIGO Scientific Collaboration & Virgo Collaboration (2017k, 2017l), (I) LIGO Scientific Collaboration & Virgo Collaboration (2017m), (J) LIGO Scientific Collaboration & Virgo Collaboration (2017n, 2017o), (K) LIGO Scientific Collaboration & Virgo Collaboration (2017p), (L) LIGO Scientific Collaboration & Virgo Collaboration (2017q), (M) LIGO Scientific Collaboration & Virgo Collaboration (2017r), (N) LIGO Scientific Collaboration & Virgo Collaboration (2017s), (O) LIGO Scientific Collaboration & Virgo Collaboration (2017t), (P) LIGO Scientific Collaboration & Virgo Collaboration (2017u), (Q) LIGO Scientific Collaboration & Virgo Collaboration (2017b), (R) LIGO Scientific Collaboration & Virgo Collaboration (2017v), (S) LIGO Scientific Collaboration & Virgo Collaboration (2017w), (T) LIGO Scientific Collaboration & Virgo Collaboration (2017x), (U) LIGO Scientific Collaboration & Virgo Collaboration (2017d).

community for decades. The LV-EM Forum, which consists of a wiki and mailing list, allowed registered astronomers to access information about GW candidate events selected for follow-up observations.

GCN/LVC notices (i.e., LIGO/Virgo-astronomers notices) are machine-readable-computer-generated messages containing

basic information about GW candidate events (e.g., time of the event and/or a sky localization probability map) or EM counterpart candidates. For the LIGO and Virgo collaborations' alerts, three types of GCN/LVC notices were produced: *preliminary*, *initial*, and *update*, although the preliminary notices were distributed only internally within the LIGO/Virgo

collaborations, while the others were sent to all members of the LV-EM forum. There was the possibility of sending a *retraction* notice as well.

1. The *preliminary* notice contains only basic trigger information such as the trigger time (equivalent to the event UTC time), the online pipeline that generated the trigger, and the event FAR. It may also contain a skymap if one is available. It reports unvetted GW candidates and is produced $\sim 1\text{--}3$ minutes after the actual event time.
2. The *initial* notice is available $\sim 20\text{--}1000$ minutes after the event (see Table 2) and is the result of further processing and human vetting of the event (see Section 2.2). In addition to the fields provided in the *preliminary* notices, it contains a link to the first sky localization probability map and source classification information if available for CBC candidate events.
3. The *update* notice is available from hours to months after the event and reports offline and parameter estimation analysis, in terms of improved FAR and sky localization.

During O2, there were 198 individuals and groups that received one or more of the three LVC notice types by any of the distribution methods and formats (i.e., VOevents, binary socket packets, and email-based methods).

The GCN circulars are human-generated prose-style descriptions of the event or follow-up observations made. They are generally sent shortly after their associated notices. For example, the LVC team generated one or two circulars for each GW candidate event, with the first being sent $\sim 1\text{--}2$ hr after the event time. Circulars are largely used to give information about follow-up observations, characteristics of the instruments/telescopes, and EM counterpart candidates. During O2, there were 385 recipients of the LVC/astronomers private circulars.

3.3. Information Sent to Observing Partners

During O1 and O2, LIGO/Virgo notices and circulars contained basic trigger information such as the event time, corresponding online pipeline name, the list of contributing instruments (H1, L1, V1), and a sky localization probability map. In the case of CBC triggers for O2, additional information about the nature of the source (see Section 3.3.2) and its localization with distance (see Section 3.3.3) was provided.

3.3.1. Significance of the Alerts

The significance of an online GW trigger during O2 was determined primarily by its FAR. The FAR of a trigger quantifies the rate at which triggers of a given kind would be generated by an online detection pipeline from data that are void of any GW signal. Only triggers with a FAR below a pre-defined threshold were considered for EM follow-up. For the majority of O2, this threshold on FAR was once per two months (1.9×10^{-7} Hz). Thus, any trigger that was generated by an online detection pipeline which could have been generated simply by noise at a rate higher than once per two months was rejected for the EM follow-up program. The FAR estimation is specific to the pipeline that triggered the event (see Section 2.1 and Table 3 for distributed alerts and the associated FARs). In Table 2, the eight triggers that were not confirmed as confident events were reported by five different pipelines. This is consistent with the expected number of false

alarms from five pipelines in 118 days of coincident data from LIGO-Hanford, LIGO-Livingston, and Virgo (LIGO Scientific Collaboration et al. 2018).

3.3.2. Source Classification of CBC Candidate Events

In an event where at least one of the component compact objects is a neutron star, the GW event is more likely to be accompanied by an EM counterpart. A new low-latency pipeline was implemented in O2 to provide observers with a source classification for compact binary coalescences. In low latency, the earliest event information that is available to use are the point estimates. The point estimates are values of the masses (m_1, m_2), and the aligned components of spin (χ_1, χ_2) of the template that triggered to give the lowest FAR during the search. However, these point estimates have uncertainties and are expected to be offset with respect to the true component values (Finn & Chernoff 1993; Cutler & Flanagan 1994; Jaranowski & Krolak 1994; Poisson & Will 1995; Arun et al. 2005; Lindblom et al. 2008; Hannam et al. 2013; Nielsen 2013; Ohme et al. 2013). Thus, any inferences drawn purely from the point estimates are prone to detection pipeline biases. To mitigate this effect, an effective Fisher formalism, introduced in Cho et al. (2013), was employed to construct an ellipsoidal region around the triggered point. This region, called the ambiguity ellipsoid, increases the chances of including the region of the parameter space that matches best with the true parameters of the source. This ambiguity ellipsoid is populated with 1000 points (a total of 1001 points including the original point estimate) which are called the ellipsoid samples. For each ellipsoid sample, the source classification quantities are computed. The dimensionality of the ambiguity ellipsoid is determined by the number of parameters required to compute the source classification quantities.

In O2 we delivered a twofold classification, one class giving the probability that at least one neutron star is present in the binary, and the second one giving the probability that there is some baryonic mass left outside the merger remnant, i.e., the EM-Bright classification. While the first classification requires only one parameter for the inference to be conducted, namely the secondary mass component, the second classification, which is more model-dependent, potentially needs more parameters than just the secondary mass. Indeed, we adopted the EM-Bright classification method from Foucart (2012) and implemented it as in Pannarale & Ohme (2014), which uses three parameters (m_1, m_2, χ_1), the masses of the primary and secondary objects, and the aligned spin component of the primary object, respectively. The method estimates the mass remaining outside the black hole after a NS–BH merger, which includes the mass of the accretion disk, the tidal tail, and/or unbound ejecta. A 3D ambiguity ellipsoid was generated around the triggered point to enclose a region of a 90% match within its boundary. This was done in the $(\mathcal{M}_c, \eta, \chi_1)$ parameter space where $\mathcal{M}_c = (m_1 m_2)^{3/5} / (m_1 + m_2)^{1/5}$ is the chirp mass and $\eta = m_1 m_2 / (m_1 + m_2)^2$ is the symmetric mass ratio. This was achieved using infrastructure developed in Pankow et al. (2015). The fraction of ellipsoid samples with secondary mass less than $2.83 M_\odot$ constituted the first classifier, namely the probability that there is at least one neutron star in the binary.

Next, the mass left outside the black hole was computed for each ellipsoid sample using the fitting formula, Equation (8) of Foucart (2012). The fraction of ellipsoid samples for which this

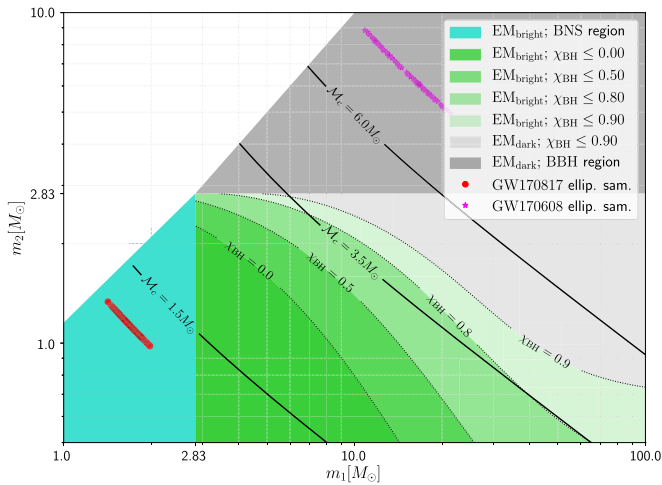


Figure 1. This figure shows the different regimes of operation by the source classifier used in O2. The BNS region is given by $(m_1, m_2) \in (0, 2.83)M_\odot$ (cyan). The upper limit of $2.83M_\odot$ is the maximum NS mass allowed by the 2H equation of state Kyutoku et al. (2010) used in the source classification software. Any system lying in this region is always considered to have an EM counterpart. The region $m_1 > 2.83M_\odot$ with $m_2 \leq 2.83M_\odot$ is the NS–BH region of the source classifier. The baryonic mass left outside the BH is computed in this region. In this scheme, the presence of any such matter is considered to provide the potential for an EM counterpart. This boundary of zero mass left outside the final BH is a function of the spin of the system. Increasing spin implies the increased possibility of an EM counterpart. Dotted contours, tagged by different χ_{BH} values, indicate the EM-bright/dark boundary, with the bright region shaded for that particular χ_{BH} value. The chirp mass, $\mathcal{M}_c = (m_1 m_2)^{3/5} / (m_1 + m_2)^{1/5}$, is the most accurately measured quantity from the GW waveform. A few chirp mass contours, $\mathcal{M}_c = (1.5, 3.5, 6.0)M_\odot$, are overlaid as solid lines for comparison. Ellipsoid samples corresponding to a BBH merger, GW170608, and a BNS merger, GW170817, are also displayed, showing consistent results with the source classifier.

was greater than zero was calculated. This constituted the second classifier.

It is important to note that Foucart’s fitting formula is only valid in the NS–BH region of the parameter space. In O2, we made the assumption that BNS mergers always emit EM radiation (i.e., EM-Bright: 100%) and BBH mergers are always void of such emission (i.e., EM-Bright: 0%, or equivalently, EM-Dark). Thus, the second classifier was computed only for ellipsoid samples with one component mass less than $2.83M_\odot$.

In Figure 1, we can see different regions of the parameter space where the aligned spin component has been suppressed and only the mass values are shown. The blue region is the BNS parameter space where every ellipsoid sample is treated as EM-Bright. The dark gray region depicts the BBH parameter space where all ellipsoid samples are treated as EM-Dark. The light gray and green shaded regions are the NS–BH part of the parameter space where the EM-Bright probability is computed using Foucart’s fitting formula. The green shaded regions show at which part of this parameter space the ellipsoid samples will give non-zero remnant mass outside the final black hole. The various shades of green discriminate between different χ_1 values, so that, for example, an ellipsoid sample with mass values $(7.0, 2.0)M_\odot$ will give non-zero remnant mass outside the black hole according to Foucart’s fitting formula if the value of χ_1 is slightly greater than 0.5, but no mass left outside the black hole below this value. Additionally, this figure also shows ellipsoid samples for GW170817. The detection pipeline point estimate for this source was consistent with a BNS system. Upon construction of the ambiguity ellipsoid around

this point estimate, we found that all the ellipsoid samples lie completely within the blue shaded region that is always assumed to be EM-Bright. In contrast, a second event that is a BBH system, GW170608, is also depicted, and its ellipsoid samples lie entirely in the EM-Dark regime.

During O2, source classification information was provided (see Table 2) on the basis of the detection pipeline within a few minutes (depending upon the component masses) of the GW detection. In the future, during the third observing run of LIGO and Virgo (O3), source classification information will be provided at multiple levels of refinement as parameter estimation results are made available.

3.3.3. Skymaps and Luminosity Distances

Currently, CBC sky localization probability maps (skymaps) for modeled searches are produced by two different algorithms, based on latency and sophistication: LALInference and BAYESTAR. LALInference uses stochastic sampling techniques for the entire parameter space of a CBC signal, such as Markov Chain Monte Carlo (MCMC) and nested sampling (Veitch et al. 2015). Kernel density estimation is applied to the posterior samples to construct a smooth probability distribution from which the sky location and distance information is calculated. Although LALInference skymaps use the most complete description of the signal, sampling is computationally expensive, with a latency ranging from hours to days and weeks. BAYESTAR circumvents this issue by utilizing the fact that most of the information related to localization is captured by the arrival time, coalescence phase, and amplitude of the signal (Singer & Price 2016).¹⁸⁶ As implemented in O2, the BAYESTAR likelihood is equivalent to that of LALInference. The marginalization is carried out via Gaussian quadratures and lookup tables. Hence, the computation can be completed within a few seconds. Due to its highly parallel nature, a typical BAYESTAR skymap is computed in 30 s.

Both LALInference and BAYESTAR provide distance information in the skymaps. The distance is estimated from the moments of the posterior distance distribution conditioned on-sky position.¹⁸⁷ In the case of LALInference the moments are calculated from a kernel density estimate trained on the posterior samples, while for BAYESTAR the moments are calculated by numerical quadrature of the posterior probability distribution.

As mentioned in Section 2.1.2, burst triggers are generated by two algorithms, cWB and oLIB, which produce their respective skymaps. The detection statistic of cWB is sensitive to the time delay in arrival of the signal at the detector sites, and thus is a function of the sky position. The skymap is constructed based on the likelihood at each point in the sky (see Klimentenko et al. 2016 for details). The oLIB skymap algorithm, LALInferenceBurst, is similar to its CBC counterpart, LALInference, in the sense of being a template-based search algorithm, except that it uses only sine-Gaussian templates. It reports a posterior in nine parameters where marginalization of parameters apart from sky position forms the skymap. Unlike CBC skymaps, burst skymaps do not contain distance information due to the lack of a signal model.

¹⁸⁶ During the late stages of O2 with the Virgo detector, more complex matched-filter S/N time series from the detection pipelines were used in place of the point estimates.

¹⁸⁷ See Section 5 of Singer et al. (2016b) for details on volume reconstruction.

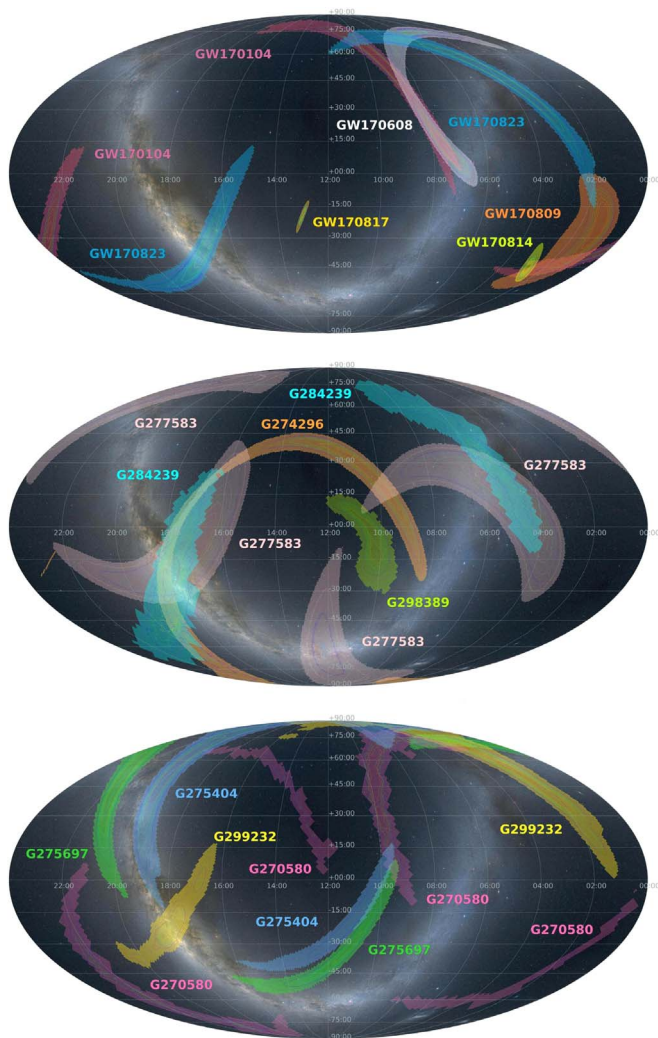


Figure 2. Distributed low-latency O2 skymaps in ICRS coordinates—Mollweide projection. The shaded areas correspond to the confidence region that encloses 90% of the localization probability. The inner lines define the target regions at a 10% confidence level with changing color scheme at every 10% increase in confidence. The upper panel shows confident events, the middle panel shows GW candidates that are consistent with noise, and the bottom panel shows the triggers rejected by the offline analysis.

Each skymap is distributed as a FITS file, a post-processed representation of the posterior samples to facilitate common queries and calculations regarding area and distance/volume when applicable. Consistent but non-numerically identical results are expected of integrals computed using FITS files versus MCMC with the posterior samples. Thus, luminosity distance medians in Table 3 and in Table 3 of LIGO Scientific Collaboration et al. (2018) differ but agree to within about 5% of the uncertainties in these quantities.

It is not unusual for both CBC and burst pipelines to identify the same astrophysical event, especially for heavier BBH mergers where the waveform is of shorter duration. In such cases, it is expected that the modeled CBC skymaps have smaller sky localizations. While there might be differences in the sky localizations, most of the probability is contained around the true location (see Vitale et al. 2017 for a comparative study).

Figure 2 shows the skymaps distributed during O2 using the low-latency algorithms discussed above. The upper panel

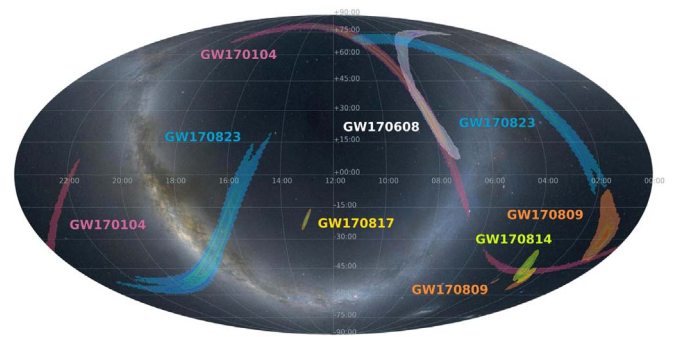


Figure 3. Offline O2 sky localizations for the confident events published in the official LIGO and Virgo catalog—Mollweide projection. The shaded areas define the 90% confidence levels. The inner lines define the target regions at a 10% confidence level, with a changing color scheme at every 10% increase in confidence.

shows the sky localizations of the high significance candidates ($\text{FAR} < 1/(100 \text{ yr}) = 3 \times 10^{-10} \text{ Hz}$), which are confident GW events. Their corresponding refined sky localizations are shown in Figure 3. Taking into account the 90% confidence region, the initial sky localizations are largely consistent with the final localizations, with GW170814 being the exception (see Section 3.3.4).

A number of candidates (principally from burst pipelines) are consistent with noise and are not considered to be GW events. These are shown in the middle panel of Figure 2. The bottom panel of the same figure shows the triggers rejected by offline analysis.

3.3.4. Three-detector Observations

The Virgo contribution to O2 is noteworthy for significantly improving the localizations of the events GW170809, GW170814 and GW170817.¹⁸⁸ As an example, for GW170814, the 50% sky localization area is confined in a single region of tens of square degrees in the southern hemisphere. We note that Virgo data was used to produce updated skymaps of GW170823 (LIGO Scientific Collaboration & Virgo Collaboration 2017d, 2017x) soon after identification of the signal. Subsequent data validation studies identified problems with the Virgo data around GW170823, which made it unreliable for use in parameter estimation: the final sky localization relies only on the LIGO data.

A note should be made regarding the initial and refined skymaps of GW170814 (Abbott et al. 2017b, 2017d): it is expected that the initial and updated skymaps for compact binary coalescence events are similar unless there are significant changes in data calibration, data quality or glitch treatment, or low-latency parameter estimations.

We observed a significant shift between the first GW170814 sky localization area and its update (LIGO Scientific Collaboration & Virgo Collaboration 2017y, 2017z). At the time of GW170814, the Virgo power spectral density (PSD) changed significantly with respect to the estimated PSD used to precompute the template bank by the GstLAL online search. Consequently, the phase of the whitening filter for Virgo was no longer canceled out by the templates. This resulted in a Virgo residual phase, which produced a phase shift in the Virgo

¹⁸⁸ Virgo data also contributed to good localization of the event GW170818 that was found by the offline search (LIGO Scientific Collaboration et al. 2018).

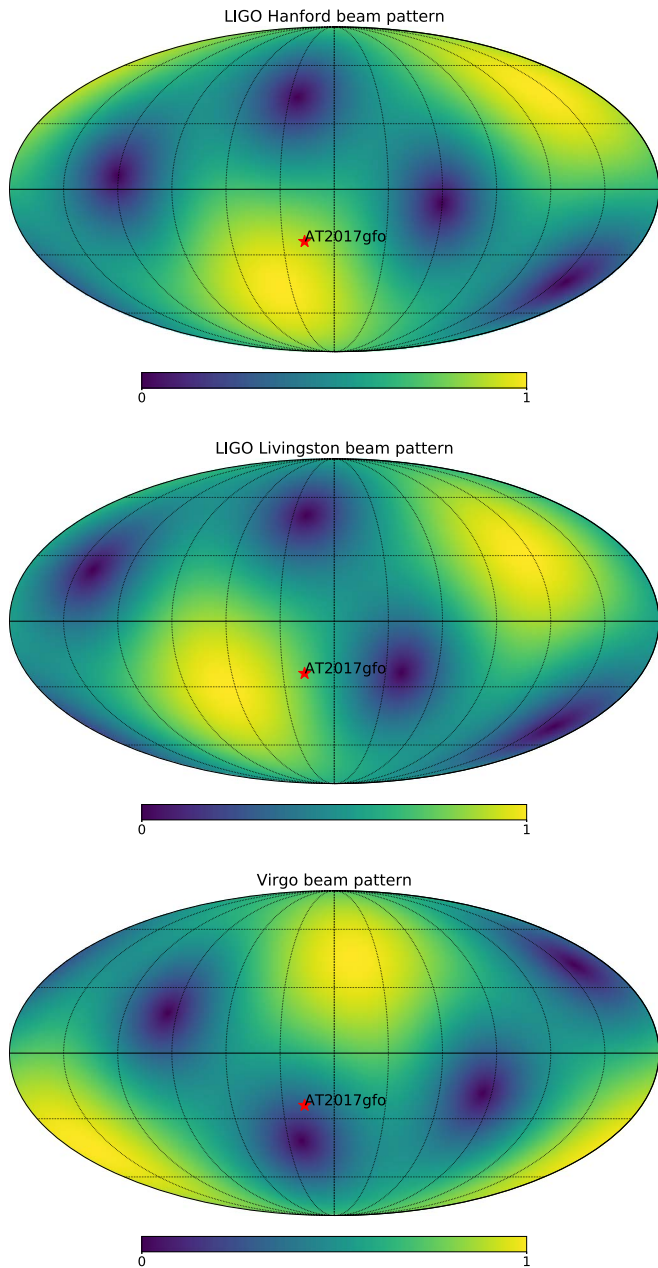


Figure 4. Antenna patterns of the GW detectors in the network at the time of the GW170817 event. Upper panel: LIGO-Hanford. Middle panel: LIGO-Livingston. Bottom panel: Virgo. ICRS coordinates—Mollweide projection. The position of the optical transient AT 2017gfo is indicated with a red star. The color indicates the strength of the response, with yellow being the strongest and blue being the weakest. At the location of GW170817, the antenna pattern amplitude for V is 2.5 to 3 times lower than that for H and L.

S/N time series causing an east shift of the 50% credible region of the sky localization area.

The antenna patterns for the three detectors are shown in Figure 4. The patterns represent the sensitivity of a detector to an event on the sky. The generic L-shaped detectors are most sensitive to signals coming from a direction perpendicular to the plane of its arms; this explains the two antipodal regions of maximum sensitivity. The plane of the arms of the detector form the least sensitive region. In this plane, the detectors are insensitive to the signal if directed along a diagonal of the L shape giving four islands of insensitivity.

3.4. Electromagnetic/Neutrino Follow-up Activity of Gravitational-wave Alerts

Searches for electromagnetic/neutrino counterparts employed a variety of observing strategies, including archival analysis, prompt searches with all-sky instruments, wide-field tiled searches, targeted searches of potential host galaxies, and deep follow-up of individual sources. They took into account the properties of the instruments, their observational capabilities (e.g., location on Earth for ground-based telescopes, pointing strategy for space-based instruments), and the characteristics of possible counterparts within their sensitivity band. For instance, the GW170817/GRB 170817A observational campaign perfectly illustrates the different observing strategies that led to the identification of the associated multiwavelength electromagnetic emission: the independent identification of the sGRB by Fermi, the all-sky archival searches and wide field-of-view follow-up, the discovery of the host galaxy and the optical GW counterpart by galaxy catalog targeted searches, the spectroscopic characterization of the optical counterpart, and the identification of X-ray and radio counterparts with deep follow-up (Abbott et al. 2017e). Similar strategies were applied to the other triggers sent in O2, but on a more modest scale.

All-sky searches. Using temporal and spatial information, the large survey instruments (thousands of square degrees, up to over half of the sky) matched their independent transient database with the GW event or performed sub-threshold investigation near the trigger time and localization area of GW events. These strategies were used by neutrino detectors (ANTARES and IceCube, Bartos et al. 2017; Dornic et al. 2017), and high-energy instruments like HAWC, *Fermi*/GBM, CGBM/Calet, *Swift*/BAT, *AstroSAT*/CZTI, and *INTEGRAL* (Martinez-Castellanos & Smith 2017; Sakamoto et al. 2017; Barthelmy et al. 2017; Bhalerao et al. 2017; Ferrigno et al. 2017; Hamburg et al. 2017; Xiong et al. 2017). Wide-field optical survey data like SVOM/mini-GWAC (Wu et al. 2017), Pan-STARRS (Smartt et al. 2017a), and iPTF (Kasliwal et al. 2017), provided pre-merger images and for prompt/early emission. The time window around the GW candidate used to search for the EM counterpart is defined on the basis of the type of GW event and the counterpart properties expected in a specific band. For GRBs, it typically covered a few seconds to minutes. In the case of neutrinos, a window of ± 500 s around the merger was used to search for neutrinos associated with prompt and extended gamma-ray emission (Baret et al. 2011), and a longer 14 day time window after the GW detection to cover predictions of longer-lived emission processes (Fang & Metzger 2017).

Tiled and galaxy catalog targeted searches. The LIGO/Virgo alerts enabled EM follow-up campaigns by scanning large portions of the gravitational-wave sky localization error box or by targeting galaxies located within it (Gehrels et al. 2016). In the case of CBC triggers, the 3D sky-distance maps (see Section 3.3.3) were used to set observational strategies using the available galaxy catalogs (LIGO Scientific Collaboration et al. 2012; Nissanke et al. 2013b; Hanna et al. 2014). Other strategies were also employed, such as, for example, selecting strong-lensing galaxy clusters that lie within the 90% credible region (GLGW Hunters Smith et al. 2017). This early follow-up of gravitational waves generally lasted tens of hours after the alert with observations from X-ray telescopes (such as *Swift*/XRT Evans et al. 2017 and

MAXI/GSC Sugita et al. 2017), as well as ground-based telescopes (e.g., MASTER, Lipunov et al. 2017; PAN-STARRs, Smartt et al. 2017b; DESGW/DECam, Soares-Santos et al. 2017; GRAWITA/REM, Davanzo et al. 2017; J-GEM/Subaru Hyper Suprime-Came Utsumi, et al. 2017; GRAWITA/VST, Greco et al. 2017; Las Cumbres/2-m, Hosseinzadeh et al. 2017; KU/LSGT, Im et al. 2017; Pirate/0.43 cm Roberts et al. 2017).

Deep follow-up and classification of the counterpart candidates. After identification of potential counterparts, further classification was pursued with narrow field-of-view and sensitive instruments. The large numbers of candidates and limited availability of larger instruments were two of the difficulties in counterpart identification.

During the O2 follow-up campaign, most of the X-ray and optical candidates were classified through spectroscopic observations that identified contaminants such as Galactic novae, supernovae, and active galactic nuclei (see, e.g., the observation campaign of GW170814 campaign by Copperwheat et al. 2017).¹⁸⁹

During the GW170104 follow-up campaign, the ATLAS survey reported a rapidly fading optical source called ATLAS17aeu in coincidence with the GW skymaps, ~ 21.5 hr after the GW trigger time. Deeper investigations with a collective approach demonstrated that ATLAS17aeu was the afterglow of a long, soft gamma-ray burst GRB 170105A, unrelated with GW170104 (Bhalerao et al. 2017; Stalder et al. 2017; Melandri et al. 2018). This was an example where a coordinated follow-up of a GW event led to a serendipitous observation of an unrelated interesting event in time-domain astronomy.

Long-term follow-up. The long-term follow-up of gravitational waves is also indispensable. One of the main challenges in radio follow-up of GW events is the association of the counterpart candidate found in the GW source localization region with the GW event, primarily due to a lack of temporal coincidence (Hotokezaka & Piran 2015; Palliyaguru et al. 2016). However, the science return is potentially immense for such long-term follow-up. For example, long-term X-rays, optical, and radio monitoring of GW170817 provided constraints on jet emission scenarios and models (Hotokezaka et al. 2016; Haggard et al. 2017; Hallinan et al. 2017b; Mooley et al. 2017; Ghirlanda et al. 2018; Margutti et al. 2018).

Figure 5 summarizes the exchange of information between LIGO/Virgo and observing partners showing the extensive follow-up activity. More than 20 circulars were generated during each follow-up campaign. From Table 3, we note that the two oLIB events (G284239 and G298389) were the least followed due to their lower significance and higher latency in delivery of the initial skymaps. Also, more than 40 GCNs were generated for GW candidates that included a neutron star as one of the binary components (G275404, G275697, G298048, and G299232). G299232 was more extensively followed due to its classification as a potential NS–BH, compared to confident detections like GW170814 or GW170608, which were BBH coalescences. This underscores the importance of source classification during O3, when observers might want to allocate their valuable resources in the most efficient manner possible.

From the EM follow-up activity side, no significant counterpart associated with BBH events was discovered; the

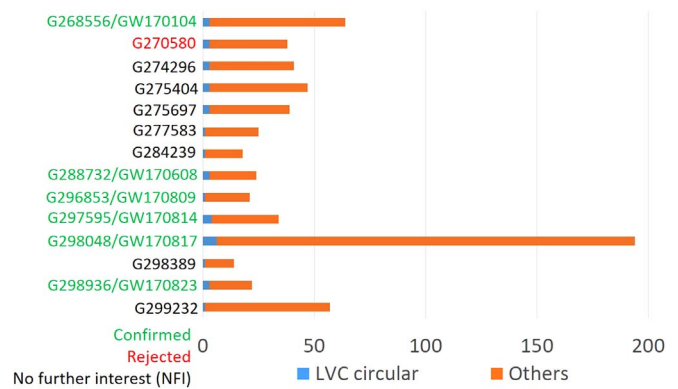


Figure 5. Summary of the exchange of information between LIGO/Virgo and its partners showing the extensive follow-up activity. The color code for the alerts refers to the status of the alerts (confident, rejected, no further interest triggers).

most promising candidate was a weak gamma-ray transient found by AGILE during GW170104 lasting 32 ms and occurring 0.5 s before the GW event (Verrecchia et al. 2017) but not confirmed by other instruments.

4. Conclusion

The O2 follow-up campaign of GW candidate events was a comprehensive effort of collaborating groups in astronomy and astroparticle physics. This effort was enabled by GW alerts distributed by the LIGO and Virgo collaborations. The triggers were produced by modeled searches for compact binary coalescences and unmodeled searches for transients such as the core-collapse of massive stars or neutron star instabilities.

During O2, 14 alerts were distributed with latencies ranging from 22 minutes up to 16 hr, most of them in less than an hour. Six events were declared as confident GW events associated with the merger of black holes or neutrons stars. The latency in sending alerts was dominated by human vetting of the candidate, which was necessary to validate data quality information beyond the ability of automated checks being in place. O2 alerts, with FARs less than one per two months, were distributed via the private GCN and contained GW information required for an efficient follow-up: the event time, sky localization probability map, and estimated FARs. For compact binary merger candidates, skymaps with a third dimension (distance), the probability of the system to contain a neutron star and the probability to be electromagnetically bright, were provided. The sky localization area of distributed events, which was hundreds to thousands of square degrees with the two LIGO interferometers, was dramatically reduced at the end of the campaign with the inclusion of Virgo.

The O2 follow-up program enabled the first combined observation of a neutron-star merger in gravitational waves (GW170817), gamma-rays (GRB 170817A), and at optical wavelengths (AT 2017gfo). Together with the identification of the host galaxy and the subsequent observations of the X-ray and radio counterparts, the data collected on this event have yielded multiple groundbreaking insights into kilonova physics, the origin of heavy elements, the nature of neutron-star matter, cosmology, and basic physics. The success of GW170817 and the larger O2 follow-up campaign demonstrates the importance of a coordinated multiwavelength follow-up program for O3 and beyond.

¹⁸⁹ <https://gcn.gsfc.nasa.gov/other/G297595.gcn3>

Future priorities of the LIGO/Virgo Collaborations include further reduction in the latency of GW alerts. The first hours after BNS mergers are crucial for observing the early X-ray, UV, and optical emissions with space- and ground-based instruments. For example, in the case of GW170817, the five hour delay in distributing skymaps, due to human intervention required to window out a glitch in LIGO-Livingston data, prevented the discovery of early emission, which could have revealed more about the the merger remnant and emission processes.

Beginning with the O3 observing run, LIGO and Virgo will issue public alerts.¹⁹⁰ There will be automated *preliminary* notices generated based on the low-latency analysis. The FAR threshold for issuing *preliminary* notices will be set so that it yields alerts with high confidence (at the level of 90%) of having an astrophysical origin for GW source types with populations that have been reliably measured until now. For other transient sources that have not been detected yet, the threshold will be lower, at the level of 1 per year. These will be followed by human-vetted *initial* notices or *retraction* notices with a latency on the order of tens of minutes for high-interest candidates and within hours for more routine detections. We expect an increase in the number of GW events; BBH merger candidates will dominate by one order of magnitude from a few per week to a few per month, whereas the BNS coalescence candidates are anticipated to occur a few times per year (Abadie et al. 2010; Abbott et al. 2016c, 2017d, 2018b, LIGO Scientific Collaboration et al. 2018). Both the increase in the number of significant candidate events and the need to reduce the latency of sending alerts will require an updated alert distribution infrastructure with a nearly fully-automated vetting protocol.


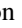
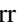








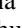
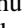

We have detailed the transient identification and alert systems utilized during the second LIGO/Virgo observing run. This work played a crucial role in ushering in the era of gravitational-wave multimessenger astronomy.

The authors gratefully acknowledge the support of the United States National Science Foundation (NSF) for the construction and operation of the LIGO Laboratory and Advanced LIGO as well as the Science and Technology Facilities Council (STFC) of the United Kingdom, the Max-Planck-Society (MPS), and the State of Niedersachsen/Germany for support of the construction of Advanced LIGO and construction and operation of the GEO600 detector. Additional support for Advanced LIGO was provided by the Australian Research Council. The authors gratefully acknowledge the Italian Istituto Nazionale di Fisica Nucleare (INFN), the French Centre National de la Recherche Scientifique (CNRS) and the Foundation for Fundamental Research on Matter supported by the Netherlands Organisation for Scientific Research, for the construction and operation of the Virgo detector and the creation and support of the EGO consortium. The authors also gratefully acknowledge research support from these agencies as well as by the Council of Scientific and Industrial Research of India, the Department of Science and Technology, India, the Science & Engineering Research Board (SERB), India, the Ministry of Human Resource Development, India, the Spanish Agencia Estatal de Investigación, the Vicepresidència i Conselleria d'Innovació Recerca i Turisme

and the Conselleria d'Educació i Universitat del Govern de les Illes Balears, the Conselleria d'Educació Investigació Cultural i Esport de la Generalitat Valenciana, the National Science Centre of Poland, the Swiss National Science Foundation (SNSF), the Russian Foundation for Basic Research, the Russian Science Foundation, the European Commission, the European Regional Development Funds (ERDF), the Royal Society, the Scottish Funding Council, the Scottish Universities Physics Alliance, the Hungarian Scientific Research Fund (OTKA), the Lyon Institute of Origins (LIO), the Paris Île-de-France Region, the National Research, Development and Innovation Office Hungary (NKFIH), the National Research Foundation of Korea, Industry Canada and the Province of Ontario through the Ministry of Economic Development and Innovation, the Natural Science and Engineering Research Council Canada, the Canadian Institute for Advanced Research, the Brazilian Ministry of Science, Technology, Innovations, and Communications, the International Center for Theoretical Physics South American Institute for Fundamental Research (ICTP-SAIFR), the Research Grants Council of Hong Kong, the National Natural Science Foundation of China (NSFC), the Leverhulme Trust, the Research Corporation, the Ministry of Science and Technology (MOST), Taiwan, and the Kavli Foundation. The authors gratefully acknowledge the support of the NSF, STFC, MPS, INFN, CNRS, and the State of Niedersachsen/Germany for provision of computational resources.

This article has been assigned the document number LIGO-P1800255.

ORCID iDs

I. Bartos  <https://orcid.org/0000-0001-5607-3637>
 P. Charlton  <https://orcid.org/0000-0003-0710-1712>
 W. M. Farr  <https://orcid.org/0000-0003-1540-8562>
 D. E. Holz  <https://orcid.org/0000-0002-0175-5064>
 V. Kalogera  <https://orcid.org/0000-0001-9236-5469>
 D. Keitel  <https://orcid.org/0000-0002-2824-626X>
 P. Koch  <https://orcid.org/0000-0003-2777-5861>
 P. D. Lasky  <https://orcid.org/0000-0003-3763-1386>
 K. Lee  <https://orcid.org/0000-0003-3175-1336>
 M. E. Lower  <https://orcid.org/0000-0001-9208-0009>
 Javed Rana  <https://orcid.org/0000-0001-5605-1809>
 Shubhanshu Tiwari  <https://orcid.org/0000-0003-1611-6625>
 J. T. Whelan  <https://orcid.org/0000-0001-5710-6576>
 Hang Yu  <https://orcid.org/0000-0002-6011-6190>

References

- Abadie, J., Abbott, B. P., Abbott, R., et al. 2010, *CQGra*, 27, 173001
 Abbott, B. P., Abbott, R., Abbott, T. D., et al. 2016a, *PhRvL*, 116, 131103
 Abbott, B. P., Abbott, R., Abbott, T. D., et al. 2016b, *PhRvL*, 116, 061102
 Abbott, B. P., Abbott, R., Abbott, T. D., et al. 2016c, *PhRvX*, 6, 041015
 Abbott, B. P., Abbott, R., Abbott, T. D., et al. 2016d, *PhRvL*, 116, 241103
 Abbott, B. P., Abbott, R., Abbott, T. D., et al. 2016e, *ApJL*, 826, L13
 Abbott, B. P., Abbott, R., Abbott, T. D., et al. 2016f, *CQGra*, 33, 134001
 Abbott, B. P., Abbott, R., Abbott, T. D., et al. 2017a, *ApJL*, 851, L35
 Abbott, B. P., Abbott, R., Abbott, T. D., et al. 2017b, *PhRvL*, 119, 141101
 Abbott, B. P., Abbott, R., Abbott, T. D., et al. 2017c, *PhRvL*, 118, 221101
 Abbott, B. P., Abbott, R., Abbott, T. D., et al. 2017d, *PhRvL*, 119, 161101
 Abbott, B. P., Abbott, R., Abbott, T. D., et al. 2017e, *ApJL*, 848, L12
 Abbott, B. P., Abbott, R., Abbott, T. D., et al. 2017f, *Natur*, 551, 85
 Abbott, B. P., Abbott, R., Abbott, T. D., et al. 2017g, *ApJL*, 848, L13
 Abbott, B. P., Abbott, R., Abbott, T. D., et al. 2018a, *CQGra*, 35, 065010
 Abbott, B. P., Abbott, R., Abbott, T. D., et al. 2018b, *LRR*, 21, 3
 Abbott, B. P., Abbott, R., Abbott, T. D., et al. 2019, *PhRvX*, 9, 011001

¹⁹⁰ <https://emfollow.docs.ligo.org/userguide/index.html>

- Acernese, F., Agathos, M., Agatsuma, K., et al. 2015, *CQGra*, **32**, 024001
- Adams, T., Buskulic, D., Germain, V., et al. 2016, *CQGra*, **33**, 175012
- Andreoni, I., D’Avanzo, P., Campana, S., et al. 2016, *A&A*, **587**, A147
- Arun, K. G., Iyer, B. R., Sathyaprakash, B. S., & Sundararajan, P. A. 2005, *PhRvD*, **71**, 084008
- Baret, B., Bartos, I., Bouhou, B., et al. 2011, *Aph*, **35**, 1
- Barthelmy, S., Lien, A. Y., Palmer, D. M., et al. 2017, GCN, 21622
- Bartos, I., Countryman, S., Finley, C., et al. 2017, GCN, 20861
- Berger, E. 2014, *ARA&A*, **52**, 43
- Bhalerao, V., Kasliwal, M. M., Bhattacharya, D., et al. 2017, GCN, 20648
- Bhalerao, V., Kasliwal, M. M., Bhattacharya, D., et al. 2017, *ApJ*, **845**, 152
- Bionta, R. M., Blewitt, G., Bratton, C. B., et al. 1987, *PhRvL*, **58**, 1494
- Biswas, R., Blackburn, L., Cao, J., et al. 2013, *PhRvD*, **88**, 062003
- Biwer, C., Barker, D., Batch, J. C., et al. 2017, *PhRvD*, **95**, 062002
- Cannon, K., Hanna, C., & Peoples, J. 2015, arXiv:1504.04632
- Cantello, M., Jensen, J. B., Blakeslee, J. P., et al. 2018, *ApJL*, **854**, L31
- Chatterji, S., Blackburn, L., Martin, G., & Katsavounidis, E. 2004, *CQGra*, **21**, S1809
- Chen, H.-Y., & Holz, D. E. 2013, *PhRvL*, **111**, 181101
- Chen, H.-Y., Vitale, S., & Narayan, R. 2018, arXiv:1807.05226
- Cho, H.-S., Ochsner, E., O’Shaughnessy, R., Kim, C., & Lee, C.-H. 2013, *PhRvD*, **87**, 024004
- Clark, J., Evans, H., Fairhurst, S., et al. 2015, *ApJ*, **809**, 53
- Copperwheat, C., Steele, I. A., Piascik, A. S., et al. 2017, GCN, 21512
- Corsi, A., & Owen, B. J. 2011, *PhRvD*, **83**, 104014
- Coulter, D. A., Kilpatrick, C. D., Siebert, M. R., et al. 2017, GCN, 21529
- Cutler, C., & Flanagan, E. E. 1994, *PhRvD*, **49**, 2658
- Dal Canton, T., & Harry, I. W. 2017, arXiv:1705.01845
- D’Avanzo, P. 2015, *JHEAp*, **7**, 73
- D’Avanzo, P., Campana, S., Ghisellini, G., et al. 2018, arXiv:1801.06164
- Davanzo, P., D’Avanzo, G. G., Melandri, A., et al. 2017, GCN, 21495
- Davis, D., Massinger, T. J., Lundgren, A. P., et al. 2018, arXiv:1809.05348
- Dobie, D., Kaplan, D. L., Murphy, T., et al. 2018, arXiv:1803.06853
- Dominik, M., Berti, E., O’Shaughnessy, R., et al. 2015, *ApJ*, **806**, 263
- Domic, D., Ageron, M., Baret, B., et al. 2017, GCN, 209866
- Eichler, D., Livio, M., Piran, T., & Schramm, D. N. 1989, *Natur*, **340**, 126
- Ensmann, L., & Burrows, A. 1992, *ApJ*, **393**, 742
- Espinoza, C. M., Lyne, A. G., Stappers, B. W., & Kramer, M. 2011, *MNRAS*, **414**, 1679
- Essick, R., Blackburn, L., & Katsavounidis, E. 2013, *CQGra*, **30**, 155010
- Evans, P. A., Kennea, J. A., Barthelmy, S. D., et al. 2017, GCN, 21503
- Evans, P. A., Cenko, S. B., Kennea, J. A., et al. 2017, *Sci*, **358**, 1565
- Falk, S. W., & Arnett, W. D. 1977, *ApJS*, **33**, 515
- Fang, K., & Metzger, B. D. 2017, *ApJ*, **849**, 153
- Ferrigno, C., Savchenko, V., Mereghetti, S., et al. 2017, GCN, 20496
- Finn, L. S., & Chernoff, D. F. 1993, *PhRvD*, **47**, 2198
- Foucart, F. 2012, *PhRvD*, **86**, 124007
- Gehrels, N., Cannizzo, J. K., Kanner, J., et al. 2016, *ApJ*, **820**, 136
- Ghirlanda, G., Salafia, O. S., Paragi, Z., et al. 2018, arXiv:1808.00469
- Goldstein, A., Veres, P., Burns, E., et al. 2017, *ApJL*, **848**, L14
- Gossan, S. E., Sutton, P., Stuver, A., et al. 2016, *PhRvD*, **93**, 042002
- Greco, G., Grado, A., Getman, F., et al. 2017, GCN, 21498
- Guidorzi, C., Margutti, R., Brout, D., et al. 2017, *ApJL*, **851**, L36
- Haggard, D., Nynka, M., Ruan, J. J., et al. 2017, *ApJL*, **848**, L25
- Hallinan, G., Corsi, A., Mooley, K. P., et al. 2017a, *Sci*, **358**, 1579
- Hallinan, G., Corsi, A., Mooley, K. P., et al. 2017b, arXiv:1710.05435
- Hamburg, R., Blackburn, L., Briggs, M. S., et al. 2017, GCN, 21711
- Hanna, C., Mandel, I., & Vousden, W. 2014, *ApJ*, **784**, 8
- Hannam, M., Brown, D. A., Fairhurst, S., Fryer, C. L., & Harry, I. W. 2013, *ApJL*, **766**, L14
- Hirata, K., Kajita, T., Koshihara, M., et al. 1987, *PhRvL*, **58**, 1490
- Holz, D. E., & Hughes, S. A. 2005, *ApJ*, **629**, 15
- Hosseinzadeh, G., Arcavi, I., Zalzman, D., et al. 2017, GCN, 21860
- Hotokezaka, K., Nakar, E., Gottlieb, O., et al. 2018, arXiv:1806.10596
- Hotokezaka, K., Nissanke, S., Hallinan, G., et al. 2016, *ApJ*, **831**, 190
- Hotokezaka, K., & Piran, T. 2015, *MNRAS*, **450**, 1430
- Im, M., Choi, C., & Lee, H. M. 2017, GCN, 21885
- Jaranowski, P., & Krolak, A. 1994, *PhRvD*, **49**, 1723
- Kasen, D., Metzger, B., Barnes, J., Quataert, E., & Ramirez-Ruiz, E. 2017, *Natur*, **551**, 80
- Kasliwal, M. M., Adams, S. M., Cannella, C., et al. 2017, GCN, 20398
- Klein, R. I., & Chevalier, R. A. 1978, *ApJL*, **223**, L109
- Klimenko, S., Vedovato, G., Drago, M., et al. 2016, *PhRvD*, **93**, 042004
- Kochanek, C. S., & Piran, T. 1993, *ApJL*, **417**, L17
- Kotake, K., Sato, K., & Takahashi, K. 2006, *RPPH*, **69**, 971
- Kulkarni, S. R. 2005, arXiv:astro-ph/0510256
- Kyutoku, K., Shibata, M., & Taniguchi, K. 2010, *PhRvD*, **82**, 044049
- Li, L.-X., & Paczyński, B. 1998, *ApJL*, **507**, L59
- LIGO Scientific Collaboration, Aasi, J., Abbott, B. P., et al. 2015, *CQGra*, **32**, 074001
- LIGO Scientific Collaboration, Virgo Collaboration, Abadie, J., et al. 2012, *A&A*, **539**, A124
- LIGO Scientific Collaboration, Virgo Collaboration, Abbott, B. P., et al. 2018, arXiv:1811.12907
- LIGO Scientific CollaborationVirgo Collaboration 2017a, GCN, 21281
- LIGO Scientific CollaborationVirgo Collaboration 2017b, GCN, 21513
- LIGO Scientific CollaborationVirgo Collaboration 2017c, GCN, 21505
- LIGO Scientific CollaborationVirgo Collaboration 2017d, GCN, 21693
- LIGO Scientific CollaborationVirgo Collaboration 2017e, GCN, 20364
- LIGO Scientific CollaborationVirgo Collaboration 2017f, GCN, 20486
- LIGO Scientific CollaborationVirgo Collaboration 2017g, GCN, 20520
- LIGO Scientific CollaborationVirgo Collaboration 2017h, GCN, 20689
- LIGO Scientific CollaborationVirgo Collaboration 2017i, GCN, 21284
- LIGO Scientific CollaborationVirgo Collaboration 2017j, GCN, 20738
- LIGO Scientific CollaborationVirgo Collaboration 2017k, GCN, 20840
- LIGO Scientific CollaborationVirgo Collaboration 2017l, GCN, 20982
- LIGO Scientific CollaborationVirgo Collaboration 2017m, GCN, 20763
- LIGO Scientific CollaborationVirgo Collaboration 2017n, GCN, 20833
- LIGO Scientific CollaborationVirgo Collaboration 2017o, GCN, 20983
- LIGO Scientific CollaborationVirgo Collaboration 2017p, GCN, 20860
- LIGO Scientific CollaborationVirgo Collaboration 2017q, GCN, 21060
- LIGO Scientific CollaborationVirgo Collaboration 2017r, GCN, 21221
- LIGO Scientific CollaborationVirgo Collaboration 2017s, GCN, 21431
- LIGO Scientific CollaborationVirgo Collaboration 2017t, GCN, 21474
- LIGO Scientific CollaborationVirgo Collaboration 2017u, GCN, 21510
- LIGO Scientific CollaborationVirgo Collaboration 2017v, GCN, 21600
- LIGO Scientific CollaborationVirgo Collaboration 2017w, GCN, 21656
- LIGO Scientific CollaborationVirgo Collaboration 2017x, GCN, 21661
- LIGO Scientific CollaborationVirgo Collaboration 2017y, GCN, 21493
- LIGO Scientific CollaborationVirgo Collaboration 2017z, GCN, 21934
- Lindblom, L., Owen, B. J., & Brown, D. A. 2008, *PhRvD*, **78**, 124020
- Lipunov, V., Gorbovsky, E., Kornilov, V. G., et al. 2017, GCN, 21499
- Lynch, R., Vitale, S., Essick, R., Katsavounidis, E., & Robinet, F. 2017, *PhRvD*, **95**, 104046
- Mandel, I. 2018, *ApJL*, **853**, L12
- Margutti, R., Alexander, K. D., Xie, X., et al. 2018, arXiv:1801.03531
- Martinez-Castellanos, I., & Smith, A. J. 2017, GCN, 21448
- Melandri, A., Rossi, A., Benetti, S., et al. 2018, arXiv:1807.03681
- Mereghetti, S. 2008, *A&ARv*, **15**, 225
- Messick, C., Blackburn, K., Brady, P., et al. 2017, *PhRvD*, **95**, 042001
- Metzger, B. D. 2017, *LRR*, **20**, 3
- Mooley, K. P., Nakar, E., Hotokezaka, K., et al. 2017, arXiv:1711.11573
- Mooley, K. P., Nakar, E., Hotokezaka, K., et al. 2018a, *Natur*, **554**, 207
- Mooley, K. P., Deller, A. T., Gottlieb, O., et al. 2018b, arXiv:1806.09693
- Mukherjee, D., et al. 2018, On the bank used in Advanced LIGO’s second observing run by the GstLAL search for inspiraling compact binaries, Tech. Rep. LIGO-P1700412, LIGO Scientific Collaboration and Virgo Collaboration
- Murase, K. 2018, *PhRvD*, **97**, 081301
- Nakar, E. 2007, *PhR*, **442**, 166
- Nakar, E., & Piran, T. 2011, *Natur*, **478**, 82
- Nielsen, A. B. 2013, *CQGra*, **30**, 075023
- Nissanke, S., Holz, D. E., Dalal, N., et al. 2013a, arXiv:1307.2638
- Nissanke, S., Holz, D. E., Hughes, S. A., Dalal, N., & Sievers, J. L. 2010, *ApJ*, **725**, 496
- Nissanke, S., Kasliwal, M., & Georgieva, A. 2013b, *ApJ*, **767**, 124
- Nitz, A. H. 2018, *CQGra*, **35**, 035016
- Nitz, A. H., Dal Canton, T., Davis, D., & Reyes, S. 2018, *PhRvD*, **98**, 024050
- Nitz, A. H., Dent, T., Dal Canton, T., Fairhurst, S., & Brown, D. A. 2017, *ApJ*, **849**, 118
- Ohme, F., Nielsen, A. B., Keppel, D., & Lundgren, A. 2013, *PhRvD*, **88**, 042002
- Ott, C. D. 2009, *CQGra*, **26**, 063001
- Paczynski, B. 1986, *ApJL*, **308**, L43
- Paczynski, B. 1991, *AcA*, **41**, 257
- Palliyaguru, N. T., Corsi, A., Kasliwal, M. M., et al. 2016, *ApJL*, **829**, L28
- Pankow, C., Brady, P., Ochsner, E., & O’Shaughnessy, R. 2015, *PhRvD*, **92**, 023002
- Pannarale, F., & Ohme, F. 2014, *ApJL*, **791**, L7
- Pian, E., D’Avanzo, P., Benetti, S., et al. 2017, *Natur*, **551**, 67
- Poisson, E., & Will, C. M. 1995, *PhRvD*, **52**, 848

- Radice, D., Perego, A., Zappa, F., & Bernuzzi, S. 2018, [ApJL](#), **852**, L29
- Regimbau, T., Siellez, K., Meacher, D., Gendre, B., & Boër, M. 2015, [ApJ](#), **799**, 69
- Roberts, D., Kolb, U., & Morrell, M. 2017, GCN, 21888
- Robinet, F. 2016, Omicron: an algorithm to detect and characterize transient events in gravitational-wave detectors, Tech. Rep. VIR-0545B-14
- Ruan, J. J., Nynka, M., Haggard, D., Kalogera, V., & Evans, P. 2018, [ApJL](#), **853**, L4
- Sakamoto, T., Yoshida, A., Kawakubo, Y., et al. 2017, GCN, 20399
- Savchenko, V., Ferrigno, C., Kuulkers, E., et al. 2017, [ApJL](#), **848**, L15
- Schutz, B. F. 1986, [Natur](#), **323**, 310
- Seto, N., & Kyutoku, K. 2018, [MNRAS](#), **475**, 4133
- Siellez, K., Boer, M., Gendre, B., & Regimbau, T. 2016, arXiv:1606.03043
- Singer, L. P., & Price, L. R. 2016, [PhRvD](#), **93**, 024013
- Singer, L. P., Chen, H.-Y., Holz, D. E., et al. 2016a, [ApJL](#), **829**, L15
- Singer, L. P., Chen, H.-Y., Holz, D. E., et al. 2016b, [ApJS](#), **226**, 10
- Smartt, S., Chambers, K. C., Smith, K. W., et al. 2017a, GCN, 21488
- Smartt, S., Huber, M. E., Chambers, K. C., et al. 2017a, GCN, 20518
- Smith, G., Smith, G. P., Richard, J., et al. 2017, GCN, 21697
- Soares-Santos, M., Allam, S., Annis, J., et al. 2017, GCN, 21789
- Stalder, B., Tonry, J., Smartt, S. J., et al. 2017, [ApJ](#), **850**, 149
- Sugita, S., Kawai, N., Serino, M., et al. 2017, GCN, 21494
- Tanaka, M. 2016, [AdAst](#), 2016, 634197
- Troja, E., Piro, L., van Eerten, H., et al. 2017, [Natur](#), **551**, 71
- Usman, S. A., Nitz, A. H., Harry, I. W., et al. 2016, [CQGra](#), **33**, 215004
- Utsumi, Y., Tominaga, N., Yoshida, M., et al. 2017, GCN, 21497
- Veitch, J., Raymond, V., Farr, B., et al. 2015, [PhRvD](#), **91**, 042003
- Verrecchia, F., Tavani, M., Ursi, A., et al. 2017, [ApJL](#), **847**, L20
- Villar, V. A., Guillochon, J., Berger, E., et al. 2017, [ApJL](#), **851**, L21
- Vitale, S., & Chen, H.-Y. 2018, [PhRvL](#), **121**, 021303
- Vitale, S., Essick, R., Katsavounidis, E., Klimenko, S., & Vedovato, G. 2017, [MNRAS](#), **466**, L78
- Wu, C., Wei, J. Y., Han, X. H., et al. 2017, GCN, 20745
- Xiongs, S., Liao, J. Y., Li, C. K., et al. 2017, GCN, 21486